โครงการ

การเรียนการสอนเพื่อเสริมประสบการณ์

ชื่อโครงการ Fabrication and characterization of lead halide with the addition of caesium cation in Perovskite solar cells

ชื่อนิสิต Miss Supattra Jitsangob **เลขประจำตัว** 5833445223

ภาควิชา Physics

ปีการศึกษา 2018

คณะวิทยาศาสตร์ จุฬาลงกรณ์มหาวิทยาลัย

Fabrication and characterization of lead halide with the addition of caesium cation in Perovskite solar cells

Supattra Jitsangob

Department of Physics, Faculty of Science

Chulalongkorn University

Submitted in part fulfilment of the requirements for 2304499 Senior Project

Second Semester, Academic Year 2018

Project Title	Fabrication and characterization of lead halide with the addition of caesium cation in Perovskite solar cells
Author	Miss Supattra Jitsangob
Advisor	Assistant Professor Sojiphong Chatraphorn, Ph.D.
Department	Physics
Academic Year	2018

This report is submitted to the Department of Physics, Faculty of Physics, Chulalongkorn University, in partial of the requirements for the degree of Bachelor of Science.

This report has been approved by the committee:

Somrit Wongmanerod ..... Chairman

(Somrit Wongmanerod, Ph.D.)

Thiti Taychatanapat .....Committee

(Thiti Taychatanapat, Ph.D.)

S. Chatraphorn .....Advisor

(Assistant Professor Sojiphong Chatraphorn, Ph.D.)

Acknowledgements

I would like to express my deep gratitude to Assistant Professor Dr.Sojiphong Chatraphorn, my advisor for his helpful guidance, enthusiastic encouragement, and assistance in keeping my progress on schedule. I would also like to offer my special thanks to Miss Kwanruthai Butsriruk and Miss Boonyaluk Namnuan, Ph.D. students, for discussions and their valuable suggestions.

Finally, I am particularly grateful to my family for their support and encouragement throughout my study.

Abstract

In general, Perovskite solar cells (PSCs) have been easily degraded by moisture, high temperature, etc. Additional of inorganic cation, e.g. Cs^+ has been introduced to explore more complex compositions which also enhances the device performance and stability. In this work, PSCs with mixed organic-inorganic cations – $MA_{1-x}Cs_xPb(I_{1-y}Br_y)_3$, where MA is methyl-ammonium, are fabricated by using the two-step spin-coating process. The halide group is also a mixture of iodide and bromide for bandgap energy tuning. The PSCs of n-i-p type are based on FTO/cp-TiO_2/mp-TiO_2/Perovskite/Spiro-OMeTAD/Au architecture. The amount of Cs is varied with x = 0.03, 0.05, 0.07 and 0.09, while the amount of Br is varied with y = 0.05, 0.10, 0.15 and 0.20. Morphologies of the perovskite layers are investigated under the variations of Cs and Br. The open-circuit voltage (V_{oc}) is directly affected by the addition of Br. The best PSC obtained in this work has V_{oc} = 1.04 V, J_{sc} = 23.4 mA/cm^2, fill-factor = 64.7% and power conversion efficiency = 15.7%.

Table of contents

Page

Page

Page

List of tables

Page

List of figures

Page

Page

Page

Chapter 1

Introduction

A population growth of human affects natural resources which maintain better life of human. Nowadays, everything in our daily-life uses various sources of energy, especially electricity. We cannot reject the fact that our lives use the electrical energy to supply our needs. The natural resources are decreasing by human habits. Fossil fuel, which could not be renewed is used for convenience and launch a lot of greenhouse gases.

Renewable energy such as wind, solar energy, etc., is a better solution for reducing of greenhouse gases. One of the outstanding renewable energy is solar energy. The spectrum of light coming from the sun covers from about 250 nm to 2,500 nm in wavelength. In addition, the surface of the earth receives about 124 exa Watts or 3,850 zetta Joules per year of solar power. This number is huge enough for solar panels to convert solar energy to electrical energy for years.

There are many types of solar cell such as Si, CIGS, but one of the high potential solar cells is a Perovskites solar cell (PSC). It is among the third-generation solar cells. Due to high cost, toxicity, and limited availability of materials of the first and the second generation solar cells, third generation, has emerged. The PSCs have attracted attention because of their ever-increasing power conversion efficiency (PCE), low cost materials, and simple fabrication process.

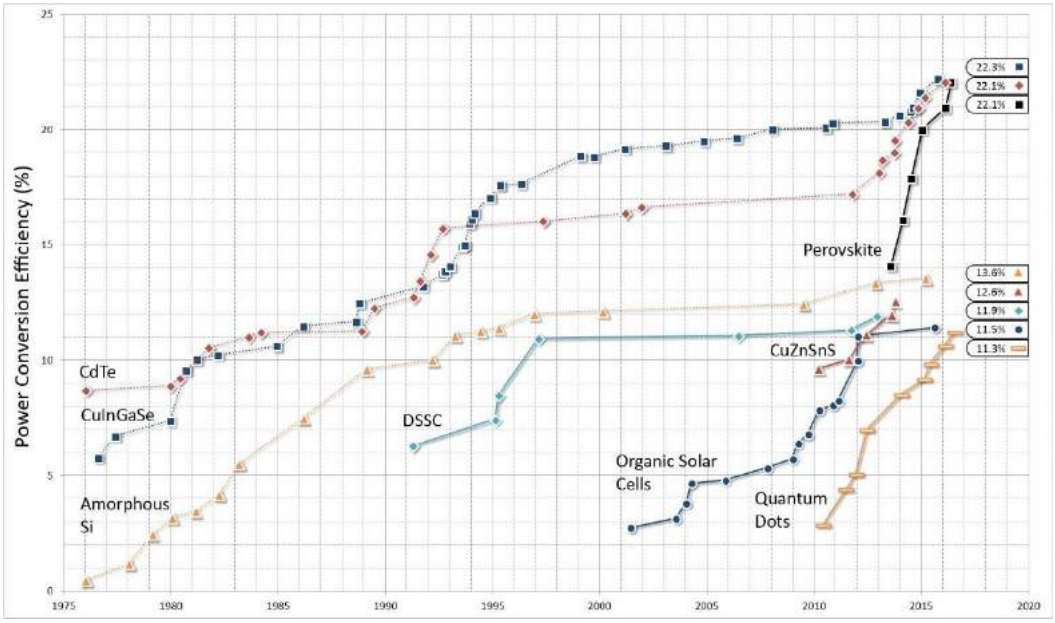

Fig.1 Power conversion efficiency of each type solar cell.
[Ref. https://www.ossila.com/pages/perovskites-and-perovskite-solar-cells-an-introduction]

First fabrication of the PSCs was in 2009 with the PCE of 3.8%, The PSCs have now achieved at a lab-scale PCE of 23.3%.[2] In addition, PSC is one of the rivaling performance for commercial multi-crystalline silicon solar cell, copper indium gallium diselenide (CIGS) and cadmium telluride (CdTe) thin film solar cells as depicted in figure1. Nowadays, PSCs can be grown on flexible and transparent materials with PCE around 23%. The flexible PSC is one of the important competitors for industrial scale.

1.1 Literature review

For many years, the instability of PSCs despite their efficiency has been known to many researchers. The original PSCs with $MAPbI_3$ have been found to be very sensitive to moisture, thermal stability, oxygen, UV light and electric field. Many researchers have studied the degradation and stability enhancement strategies to solve those problems.

According to moisture and oxygen, they can cause intermediate formation. This instability can be avoided by device encapsulation to protect the PSCs.[1],[2] Moreover, the UV-light can be avoided by adding UV filter onto the PSCs. The stability toward an electric filed can be solved by suppressing the trap state of the PSCs.[3],[4] On the other way, the thermal

stability and others can be improved in crystal structure scale by addition chemical substance.

1.1.1 Caesium (Cs) addition

Methyl-ammonium lead halide perovskite ($MAPbX_3$; X=I, Br, Cl) are among interests. Cs addition is to replace an organic cation (MA) in the $MAPbX_3$ structure with an inorganic cation. According to degradation, the Cs addition has been used to solve instabilities such as; thermal instability, phase transition and bias-induced ion migration.[2]

In addition, Cs has been used to explore more complex compositions, including Cs and MA, Cs and FA, and Cs, MA and FA which also enhance the device performance because of smaller atomic radius.[2],[5] The improvement of short-circuit current comes from the increased film thickness. However, Cs formation at room temperature is a yellow orthorhombic phase with bandgap energy (E_g) of ~2.82 eV that shows instability for solar cell applications. Upon heating, it can form a black cubic perovskite phase with E_g of ~1.73 eV.[6] It can be transformed to the black phase at temperature of ~310°C.[6] Therefore, the thermal stability can be solved by Cs addition. The Cs addition can increase not only thermal stability but also device performance.[2]

1.1.2 Bromine (Br) addition

Many studies have shown that Br^- ions tend to replace the I^- ions which are linked to the Pb^{2+} inducing modifications in the morphology of the perovskite layer. Moreover, a growth of larger grains with an enhancement of optical absorption is occurred when Br is added.

In addition, open-circuit voltage (V_{oc}) can be increased by Br addition.[5],[6] Moreover, the band gap is blue shifted by the addition of Cs and Br. The cobalt addition with both Cs and Br is another way to improve the stability and the efficiency of PSCs, while the $MAPbI_3$ PSCs still have the issue of instability of cells such as thermal instability and grain boundary.[5]

1.2 Research objectives

To study the characteristics of $MA_{1-x}Cs_xPb(I_{1-y}Br_y)_3$ PSCs which additions of Cs and Br in the light harvesting layer.

1.3 Scope of this work

In this work, PSCs with mixed organic-inorganic cations – $MA_{1-x}Cs_xPb(I_{1-y}Br_y)_3$, where MA is methyl-ammonium, are fabricated by using the two-step spin-coating process. The halide group is also a mixture of iodide and bromide for bandgap energy tuning. The PSCs of n-i-p type are based on FTO/cp-TiO_2/mp-TiO_2/Perovskite/Spiro-OMeTAD/Au architecture. The amount of Cs is varied with x = 3, 5, 7 and 9%, while the amount of Br is varied with y = 5, 10, 15 and 20%. Finally, the PSCs are measured by a UV/VIS/NIR spectrophotometer for transmittance and absorbance, a solar simulator for solar cell parameters, and a scanning electron microscope for morphologies.

1.4 Outline

There are 5 chapters in this report;

Chapter 1 Introduction and motivation

The first chapter is the explanation of the important points in this work, and the objectives of this work.

Chapter 2 Perovskite: material, solar cells, and characterization techniques.

This chapter describes the basics of perovskite and PSCs, optical properties, and the basic concepts of solar cells.

Chapter 3 Fabrication of PSCs

The preparations of PSCs are described in this chapter.

Chapter 4 Results and discussion

The results of I-V measurements, transmission, absorbance, grain size, and coloration of the cells are shown in this chapter. The results are discussed and compared between the original PSCs and the PSCs with Cs and Br additions.

Chapter 5 Conclusions

This chapter is a summary of the experiment and the important results of finding.

Chapter 2

Basics of perovskite: materials, solar cells, and characterization techniques.

There are five main parts in this chapter; perovskite materials, perovskite solar cell structure, characterization techniques, working principle of PSCs and solar cell parameters. The first part is about natural structure of perovskite and its properties. Second, PSCs and materials comprising; 1) electron transport material, 2) hole transport material, and 3) light harvesting material are described. Working principle of PSCs, solar cell parameters, and characterization techniques are respectively explained.

2.1 Perovskite materials

Perovskite is a materials with the general formula ABX_3. The natural perovskite material is calcium titanate ($CaTiO_3$). The ideal from crystal structure of cubic ABX_3 perovskite can be described as consisting of corner sharing (BX_6) octahedral with A cation occupying the 12-fold coordination site formed on the middle of the cube of eight such octahedral.[2]

In general, PSC material for solar cell applications is an inorganic-organic hybrid material with a perovskite (ABX_3) structure where A is methyl-ammonium ($CH_3NH_3^+$, MA), formamidinium (FA), Cs, B can be Pb, Sn and X is halogen ion. The ideal structure of the perovskite is cubic as shown in figure 2.

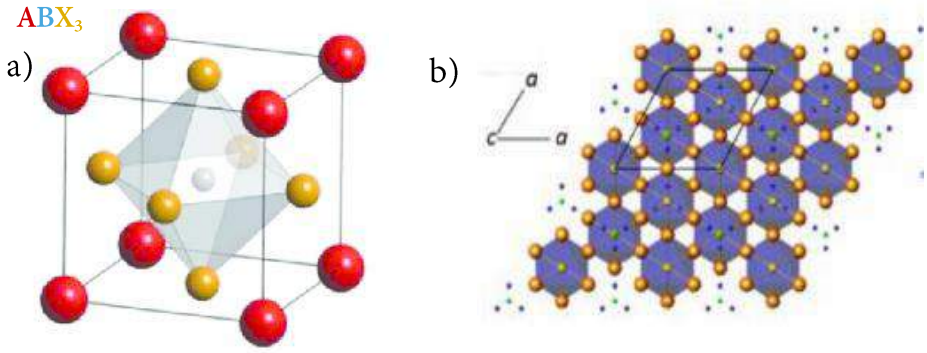

Fig.2 a) A unit cell of perovskite structure where A= methyl-ammonium ($CH_3NH_3^+$, MA), formamidinium ($HC(NH_2)_2^+$, FA), Cs or Rb, B= Pb, Sn and X= halogen ion. b) Polyhedral representations of Perovskite structure [6].

Perovskite structures are found to be sensitive to moisture, oxygen, UV light soaking, thermal instability, electric field, and other potential factors.[2] However, the moisture and oxygen instability could be avoided by device encapsulation.[6] In addition, PSCs could be protected from UV light by adding UV filters on devices. In this report we focus on Cs and Br addition in perovskite layer to study the effect on the device performance.

2.2 Perovskite solar cell structure

The PSC structure basically consists of a light harvesting layer sandwiched between electron transport material (ETM) and hole transport material (HTM). However, the most successful and extensively studied arrangement is shown in figure 3.

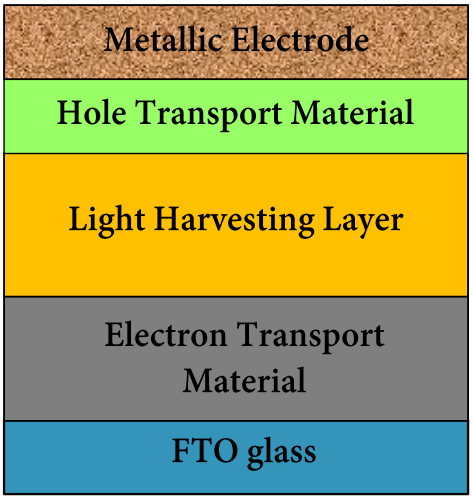

Fig.3 The structure of perovskite solar cells.

The substrate for the PSCs is fluorine-doped tin oxide (FTO) glass. Titanium dioxide (TiO_2) as the ETM is deposited on the FTO glass followed by a light harvesting layer or perovskite layer. After that an HTM such as spiro-OMeTAD is deposited on top of the absorber layer. Finally, metallic electrodes made of gold (Au) are evaporated through a shadow mask. In some devices, variations in the regular structure have been considered. e.g. FTO/HTM/perovskite/ETM/metallic-electrode and known as an invert-structure.

1. Electron transport material (ETM)

An ETM which is generally an n-type material used in PSCs is TiO_2 because of its transparency to visible light, low absorption and high refractive index. There are three types of TiO_2; rutile, anatase, and brookite. The rutile phase is thermodynamically the most stable phase while anatase is the most interesting for use in high surface area photocatalytic and PV devices. Moreover, TiO_2 has a regular structure in two main configurations in PSCs: a compact layer and a mesoporous scaffold layer. The anatase phase is used to be the ETM in this work.

2. Hole transport material (HTM)

An HTM as a p-type material is necessary for efficient extraction of holes toward metallic electrode and perfect prevention of electron across the interface. The HTM should be sufficiently thick to cover the area of the perovskite layer before deposition of metallic cathode. The HTM layer should have a thickness around 100-300 nm. In this work, spiro-OMeTAD is employed as the HTM.

3. **Light harvesting material**

Most PSCs use $MAPbI_3$ as the light harvesting material because it has been found to be a direct band-gap semiconductor with high absorption coefficient and large carrier mobility. In addition, the intrinsic electrical conductivity of $MAPbI_3$ can be modified from p-type and n-type by controlling growth condition.[5] The properties of material generally used in the PSCs are summarized in Table 1.

Table1 Materials and their properties typically used in PSCs.

Material	Role	Bandgap energy (eV)	Work function(eV)	Electron affinity(eV)	Dielectric constant
FTO	TCO	4.0-4.5	4.4-5.0	5.6	3.9
TiO_2	ETM	3.2	3.7-4.2	3.6-4.1	18-22
Spiro-OMeTAD	HTM	3.0-3.6	3.9-5.2	2.11	3.0
$MAPbI_3$	Light absorber	1.51-1.61	-	3.9-4.8	22-35
Au	electrode	-	4.3-4.4	-	-

*TCO - transparent conducting oxide.

2.3 Working principle of PSCs

The working principle of solar cells is based on the photovoltaic effect, such as the generation of a potential difference at the junction of two different materials in response to electromagnetic radiation. The photovoltaic effect is closely related to the photoelectric effect, where electrons are emitted from a material that has absorbed light with a frequency above a material-dependent threshold frequency. The energy of a photon is given by

$$E = hv, \tag{1}$$

where h is Planck's constant,

v is the frequency of light.

When the thickness of the film is known, we can obtain an optical absorption spectrum and consequently the optical band gap energy (E_g) from transmission and reflection measurements (UV/VIS spectroscopy) which is described next. Moreover, when the semiconductor is irradiated with light, photons are absorbed to generate electron-hole pairs. The absorption of solar cell can be divided into three cases as depicted in figure5;

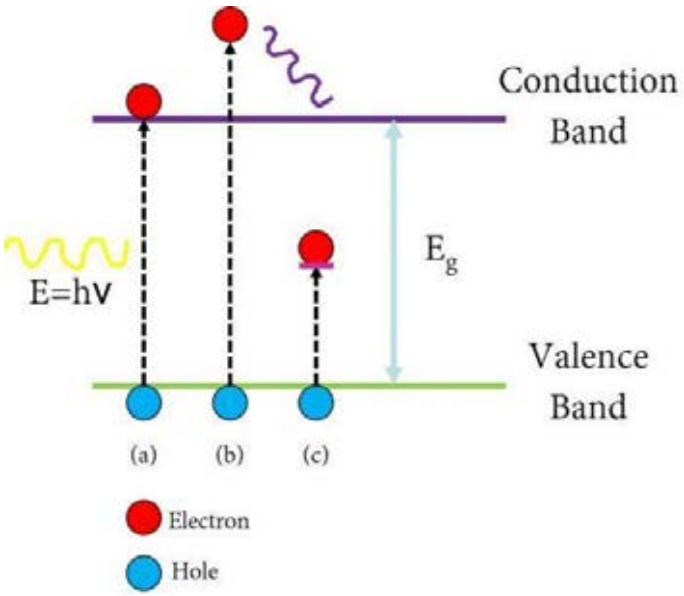

Fig.4 The absorption of semiconductor; (a) $hv = E_g$, (b) $hv > E_g$, (c)* $hv < E_g$.
For (c)* can occur when electron have energy.

(a) The photon energy is equal to E_g, a photon energy will be absorbed.

(b) The photon energy is greater than E_g, an electron-hole pair is generated. Then, the excess energy is dissipated as heat. (a) and (b) are called *"intrinsic transition or band-to-band transition"*.

(c) There are available energy states in the forbidden gap due to the physical defects, and is called *"extrinsic transition"*.

For reverse situation, an electron at the conduction band edge recombines with a hole at the valence band edge resulting in the emission of a photon with energy equal to that of the energy difference. For the band-to-band transition can be divided into two types; allowed direct transition, and forbidden direct transition.

1) Allowed direct transition

The absorption coefficient (α) is related to light frequency as the following equation;

$$\alpha(v) = \frac{A'(hv-E_g)^{1/2}}{hv}, \quad (2)$$

where A' is constant,

hv is the energy of a photon with frequency v,

E_g is band gap energy.

2) Forbidden direct transition

$$\alpha(v) = \frac{A^*(hv-E_g)^{3/2}}{hv}, \quad (3)$$

where A* is constant,

hv is the energy of a photon with frequency v,

E_g is band gap energy.

The PSCs in this work are allowed direct transition semiconductor. The absorbance and energy gap can be calculated from equation (2). We can rewrite equation (2) as

$$(\alpha hv)^2 = A'(hv - E_g) \quad (4)$$

We plotted between $(\alpha hv)^2$ as y axis and the E_g as x axis. The E_g can be obtained by the extrapolation of the linear section to the intercept on the hv axis as shown for example in figure 5. The thickness of perovskite layer was measured by SEM cross section as shown in figure 6.

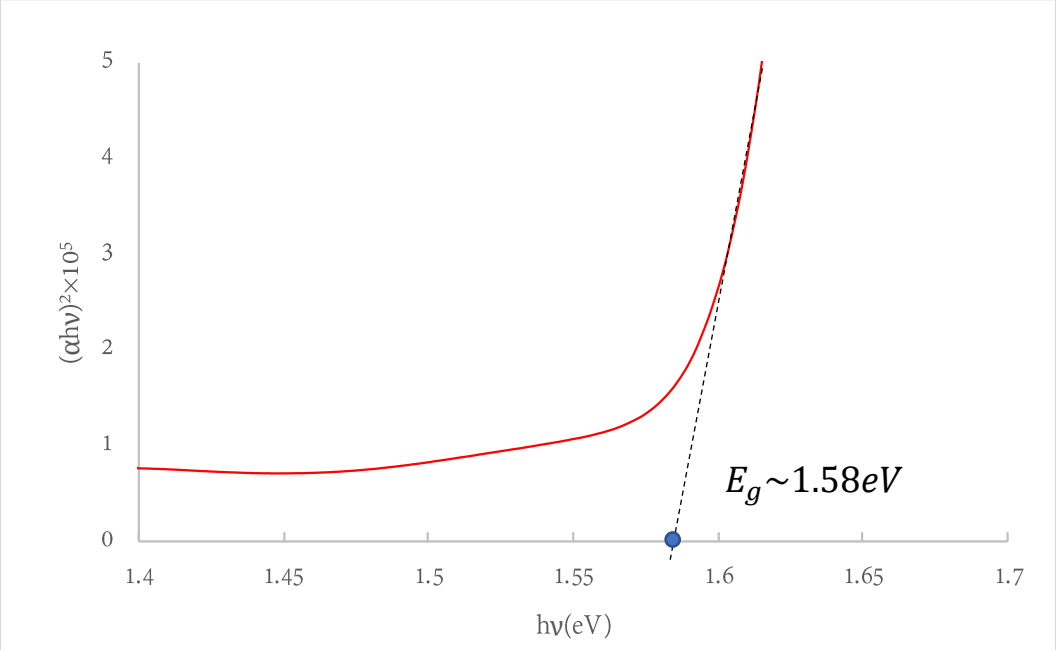

Fig.5 A plot between $(\alpha hv)^2$ and hv to find the E_g from the linear section to the intercept on the hv axis.

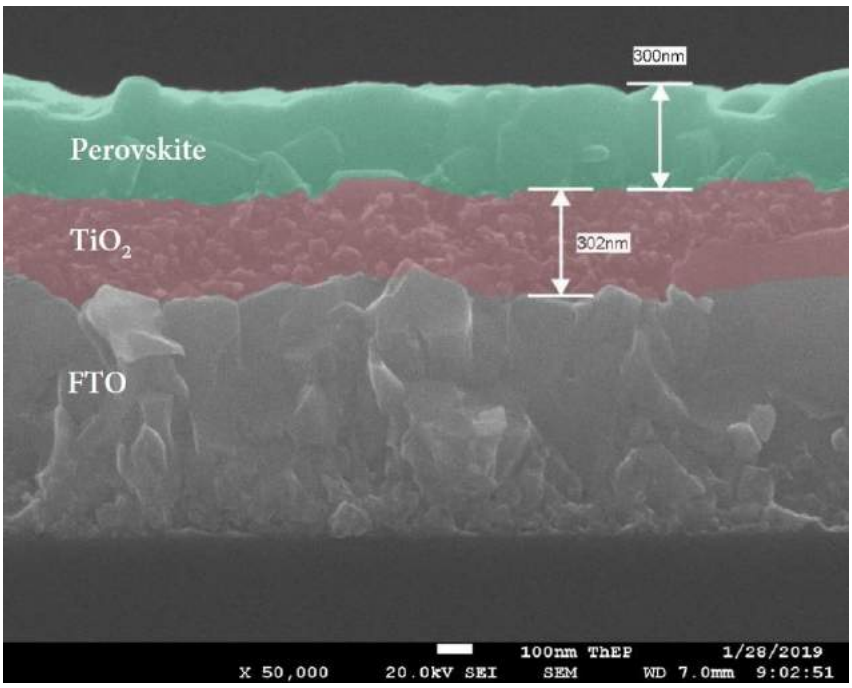

Fig.6 Thickness of Perovskite layer is 300 nm.

2.4 Solar cell parameters

When the PSCs are working, the electric current will be generated. Four solar cell parameters are investigated in this work; open-circuit voltage (V_{oc}), short-circuit current density (J_{sc}), fill factor (FF) and power conversion efficiency (PCE). The solar cell parameters are measured by I-V measurement which is described in the characterization techniques.

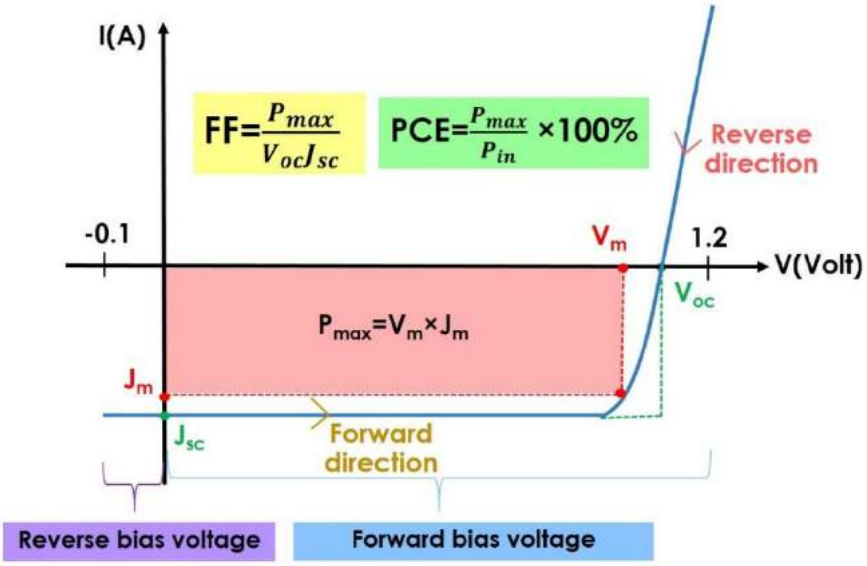

Fig.7 I-V characteristics of illuminated solar cell.

The parameters that are used to characterize the performance of the solar cells are determined from the illuminated I-V characteristic as illustrated in figure 7. There are two directions of voltage applied; forward, and reverse. The forward direction in this work is applied from -0.1 to 1.2 V. In contrast, the reverse direction is applied from 1.2 to -0.1 V to compare the I-V characteristics between the forward and reverse directions. However, the V_{oc} and J_{sc} for forward and reverse directions should be nearly the same values as shown in figure 7. A forward bias voltage is the range which has a positive value of voltage. A negative value of the applied voltage is called a reverse bias voltage.

1) Open-circuit voltage (V_{OC})

V_{oc} is the voltage at the point which no current flows through the external circuit. It is the maximum voltage that the solar cell can deliver. V_{oc} corresponds to the forward bias voltage, at which the dark current compensates the photocurrent. V_{oc} is also a measure of the amount of recombination in the device. Moreover, V_{oc} depends on the photo-generated current density and can be calculated as following equation;

$$V_{oc} = \frac{kT}{e}\ln\left(\frac{J_{ph}}{J_0} + 1\right), \quad (5)$$

where k is the Boltzmann constant,

T is temperature,

J_{ph} is the photo-generated current density,

J_0 is saturation-current density of the p-n junction.

2) Short-circuit current density (J_{sc})

J_{sc} is the current that flows through the external circuit when the electrodes of the solar cell are short circuited or at zero bias voltage. The short-circuit current of a solar cell depends on the photon flux density incident on the solar cell which is determined by the incident light. The standard solar cell measurements is standardized to AM 1.5.

The short-circuit current density is used to describe the maximum current that the solar cell can deliver and strongly depends on absorption or reflection of each layer.

3) Fill factor (FF)

FF is the ratio between the maximum power generated by a solar cell and the product of V_{oc} with J_{sc}.

$$FF = \frac{J_{mp}V_{mp}}{J_{sc}V_{oc}} = \frac{P_{max}}{J_{sc}V_{oc}}, \quad (6)$$

where J_{mp} is current density at maximum power,

V_{mp} is voltage at maximum power.

4) Power conversion efficiency (PCE)

PCE is calculated as the ratio between the maximum generated power and the incident power. The irradiance value P_{in} of 1,000 W/m^2 for the AM 1.5 spectrum has become a standard for measuring the conversion efficiency of solar cells. The conversion efficiency can be calculated as the following equation;

$$\eta = \frac{P_{max}}{P_{in}} \times 100\% = \frac{J_{mp}V_{mp}}{P_{in}} \times 100\% = \frac{J_{sc}V_{oc}FF}{P_{in}} \times 100\%. \quad (7)$$

Note that, good solar cell parameters of the PSCs are excepted to have; J_{sc} ~ 25 mA/cm^2, V_{oc} up to 1 V, and FF in the range 0.60-0.85 and PCE lies in the range of 16-23%.

2.5 Characterization techniques

In this part, there are three characterization techniques used in this work; 1) I-V measurement 2) UV/VIS/NIR spectroscopy for absorbance and transmittance, 3) scanning electron microscope (SEM) for surface morphology.

2.5.1 I-V measurement

The I-V measurement setup consists of a xenon lamp as a solar simulator, a high current source-meter unit (Keithley model 238) in a 4-point configuration. The PSCs with 0.06 cm^2 and 0.2 cm^2 active areas are

analyzed under AM1.5 condition at room temperature (25°C) with light intensity of 100mW/cm^2

2.5.2 UV/VIS/NIR spectroscopy

The basic principles; transmission and reflection of light through a semiconductor are described in this part.

1) Basic principles

Consider figure 8, a semiconductor is irradiated by a light source with intensity I_0. When the light is traveling through the semiconductor, the transmitted light I_T decreases due to the absorption process in the material.

According to the absorption, it is expressed in terms of an absorption coefficient α which is defined as the relative decreasing rate of light intensity along its propagation path;

$$\alpha = -\frac{1}{I(x)}\frac{dI(x)}{dx}. \quad (8)$$

Note that the negative sign indicates decreasing intensity of light due to absorption. The solution of equation (8) with boundary condition I(x) = I_0 at x = 0, is

$$I(x) = I_0 e^{-\alpha x}. \quad (9)$$

The transmittance (T) and the reflectance (R) can be expressed in terms of the intensity of incident light I_0, the intensity of transmitted light I_T and the intensity of reflected light I_R as

$$T = \frac{I_T}{I_0}, \quad (10)$$

$$R = \frac{I_R}{I_0}. \quad (11)$$

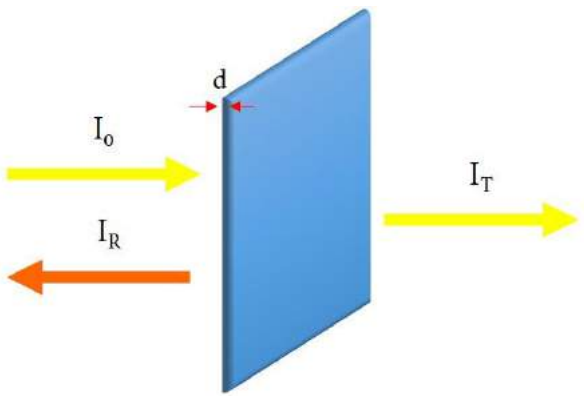

Fig.8 Transmission and reflection of light through a material.

The transmission, reflection, and absorption obey the following equation;

$$T + R + A = 1. \tag{12}$$

Equations (9) and (12) can be rewritten in the form of

$$\alpha = -\frac{1}{d}\ln\left[\frac{T}{(1-R)^2}\right]. \tag{13}$$

Equation (13) is the result of multiple reflections and transmission at both the top and bottom surfaces. However, when R is comparatively small, then

$$\alpha \approx -\frac{1}{d}\ln(T). \tag{14}$$

From figure 9, consider the thin film of a uniform thickness (d) and an index of reflection (n_f). Assume that the light rays traveling in the air are nearly normal to the surface of the film. The fundamental property of optics which the light pass through an interface between materials of different indices of reflection can be divided into transmitted and reflected components as the following facts;

1) If $n_f > n_s$ no phase change. This case is "*constructive interference*";

$$2d = m\lambda, \tag{15}$$

2) If $n_f < n_s$ undergoes a 180°, phase will change. This case is "*destructive interference*";

$$2d = (m + \frac{1}{2})\lambda, \tag{16}$$

where d is the film thickness,

λ is the wavelength,

m is a positive integer (m=1,2,3,...).

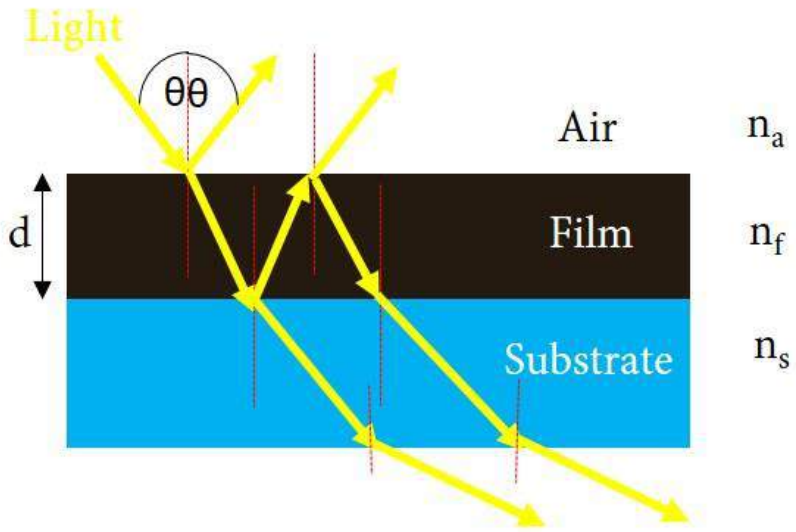

Fig.9 Schematic diagram showing optical paths for transmission and reflection through thin film.

In addition, the wavelength of light λ_n in the medium whose reflection index is

$$\lambda_n = \frac{\lambda_0}{n}, \tag{17}$$

where λ is the wavelength of the light in the free space.
Consider equation (9), It can be used to determine the film thickness through the relationship;

$$d = \frac{m\lambda_0}{2n} = \frac{(m+1)\lambda_1}{2n} = \frac{(m+i)\lambda_i}{2n}, \tag{18}$$

where i is the number of complete cycles from λ_0 to λ_i.

We obtain m from

$$m = \frac{i\lambda_i}{\lambda_0 - \lambda_i}. \tag{19}$$

Substitute equation (15) into (14);

$$d = \left(\frac{\lambda_0}{2n}\right)\left(\frac{i\lambda_i}{\lambda_0 - \lambda_i}\right). \tag{20}$$

When i=1, we obtain

$$d = \frac{\lambda_0\lambda_1}{2n(\lambda_0 - \lambda_1)} = \frac{1}{2n\left(\frac{1}{\lambda_1} - \frac{1}{\lambda_0}\right)}. \tag{21}$$

In this report, the thickness d of perovskite layer can be measured by Scanning Electron Microscope (SEM) because the reflective index of the film is not exactly known.

2) Working principle of UV/VIS/NIR spectroscopy

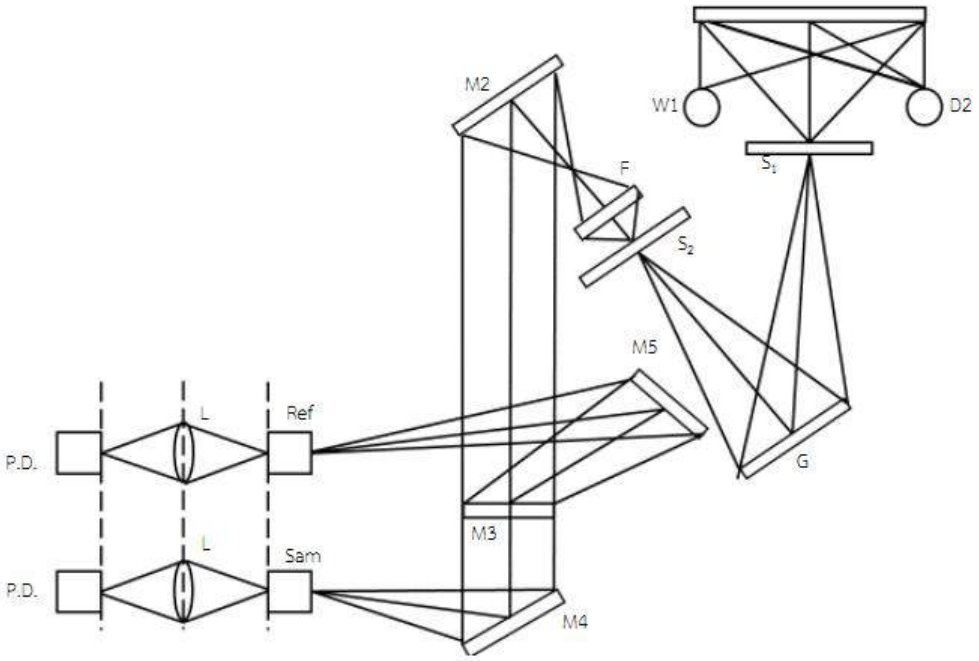

Fig.10 Schematic drawing of UV/VIS/NIR spectrophotometer. [9.]

D2: Deuterium lamp	W1: Halogen lamp
M1-M5: Mirror	M3: Half mirror
F: Filter	L: Lenses
G: Grating	Sam: Cell of sample beam
S_1: Entrance slit	Ref: Cell of reference beam
S_2: Exit slit	P.D.: Photo diode detector

Figure 10 shows the optical path of materials using the Shimadzu spectrophotometer model UV-1601PC. The spectrophotometer has built-in CPU that controls the light sources, the switching mechanisms of the light sources, the slit width, the grating, the wavelength scanning and the detector switching as shown in figure 10.

The spectrophotometer is interfaced and controlled via the external computer. Moreover, the sample and the reference beams are detected by silicon photodiodes. Then, the output from the detectors are passed to the preamplifier, the gain-amplifier and then converted into digital data by A/D converter as figure 11.

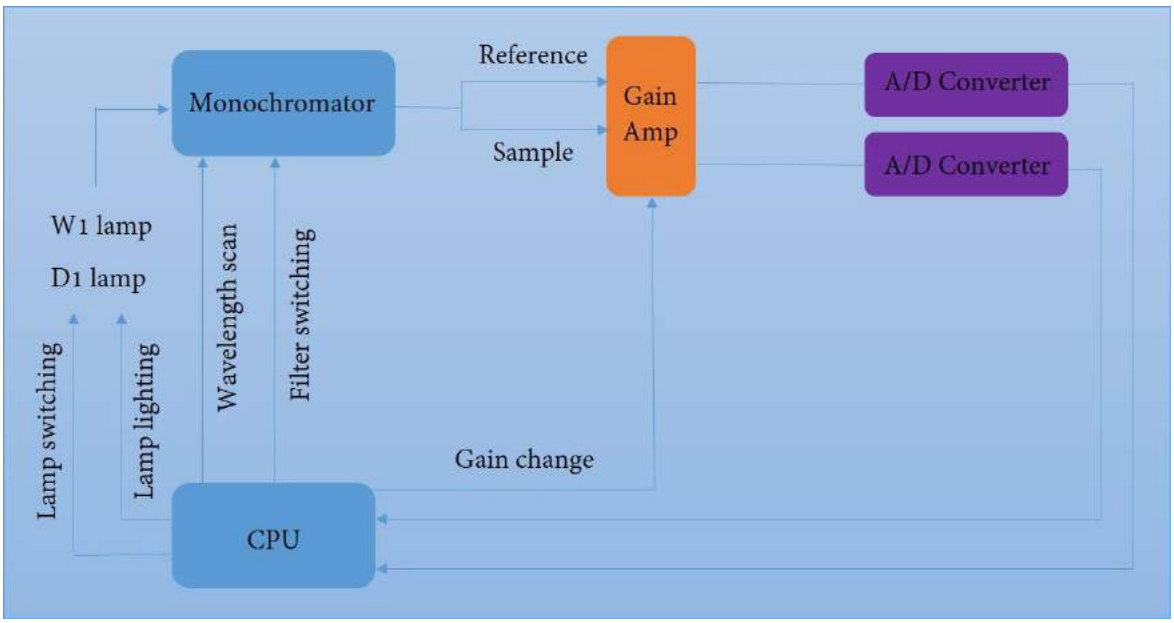

Fig.11 Schematic diagram showing the electrical system of UV-1601PC spectrophotometer.

2.5.3 Scanning Electron Microscope (SEM)

Electrons which carry significant amounts of kinetic energy are accelerated at electron source or gun in SEM. The accelerated electrons are passed through the condenser lenses to produce a focus beam of electrons which hit the sample surface as depicted in figure 12. The direction of electron beam is controlled by a set of coils. Finally, the electron-sample interactions are occurred and the signals are measured by appropriate detectors.

Moreover, the kinetic energy is dissipated as a variety of signals produced electron-sample interactions when the incident electron are decelerated in the substrates. These signals include secondary electrons that produce SEM images, backscattered electrons (BSE), diffracted backscattered electrons, photons, visible light, and heat. Secondary electrons and backscattered electrons are commonly used for imaging sample:

1) **Secondary electrons** for showing morphology and topography on samples.
2) **Backscattered electrons** for illustrating contrasts in composition in multiphase samples.

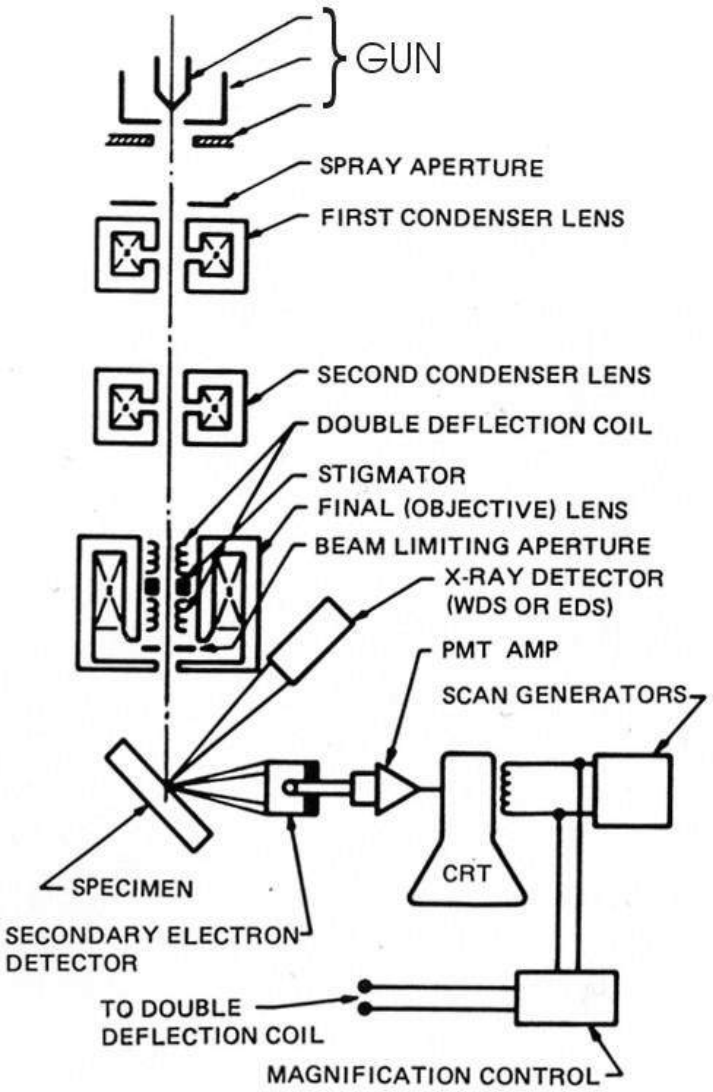

Fig.12 Schematic drawing of the scanning electron microscope.
[**Ref.**https://serc.carleton.edu/research_education/geochemsheets/techniques/SEM.html]

There are 6 essential components of SEM;

1) Electron source (GUN)
2) Electromagnetic lenses
3) Sample stage
4) Detectors
5) Data output devices

In this report, JEOL (JSM-7001F) field emission scanning electron microscope was used to observed perovskite absorbers' morphology.

Chapter 3

Fabrication of PSCs

In this chapter, the preparation of chemical substance and substrates are described. The PSCs with mixed organic-inorganic cations – $MA_{1-x}Cs_xPb(I_{1-y}Br_y)_3$, where MA is methyl-ammonium, are fabricated by using the two-step spin-coating process. The PSCs of n-i-p type are based on FTO/cp-TiO_2/mp-TiO_2/Perovskite/Spiro-OMeTAD/Au architecture. The amount of Cs is varied with x = 3, 5, 7 and 9% of Cs concentration, while the amount of Br is varied with y = 5, 10, 15 and 20% of Br concentration.

3.1 Equipment

The list of deposition and characterization tools are as followed.

3.1.1 Deposition tools

1) Branson 3510 ultrasonic bath
2) MicroNano Tools spin coater model KW-4A
3) Nitrogen air glovebox
4) Gold evaporator

3.1.2 Characterization tools

1) Solar simulator
2) I-V measurement setup
3) UV/VIS/NIR spectrophotometer; Shimadzu model UV-1601PC
4) Scanning Electron Microscope; JEOL model JSM-7001F

3.2 Preparation of substrates

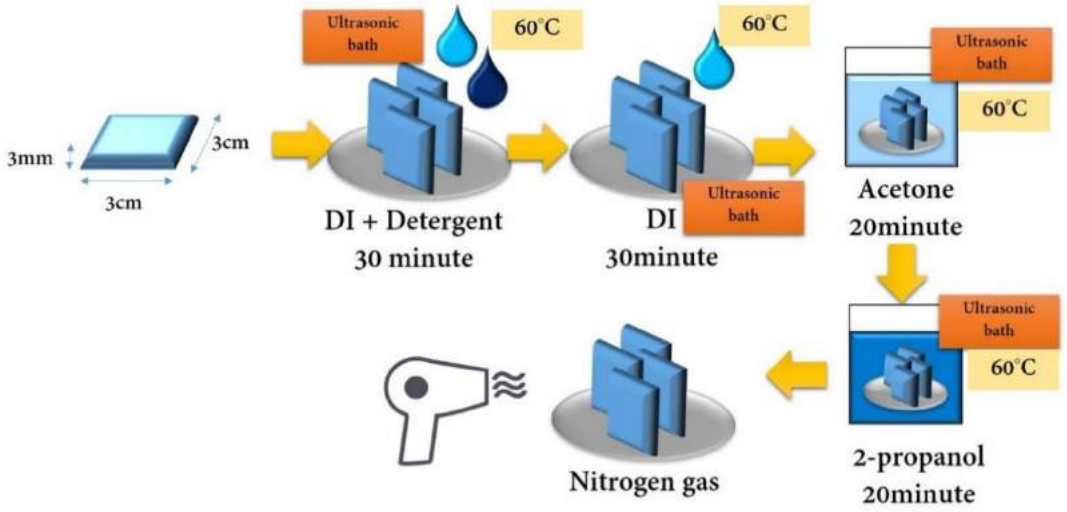

Fig.13 Substrates cleaning process.

Fluorine-doped tin oxide coated glass (FTO) (size 3×3 cm^2, thickness 3 mm) substrates were partially etched using a chemical treatment with zinc powder and 37% concentration of hydrochloric acid, cleaned with detergent and rinsed with deionized water. Then, the substrates were cleaned with acetone and IPA in an ultrasonic bath for 30-60 minutes. Finally, they were dried with compressed nitrogen gas as depicted in figure13.

3.3 Chemical preparation

This part describes a preparation of materials for the fabrication of PSCs with the conditions;

- $MAPb(I_{0.85}Br_{0.15})_3$ – as the reference sample,
- $MA_{1-x}Cs_xPb(I_{0.85}Br_{0.15})_3$ with x= 0.03, 0.05, 0.07, 0.09,
- $MA_{0.97}Cs_{0.03}Pb(I_{1-y}Br_y)_3$ with y= 0.05, 0.10, 0.15, 0.20.

The calculations of chemical substance for the reference sample with A = MA, B = Pb, and $X_3 = (I_{0.85}Br_{0.15})_3$ [0.065M] are based on 1 mol of MAI = 159 g, 1 mol of MABr = 112 g, and 1 mol of PbI_2 = 461 g.

First, the mass of each chemical substance were calculated by the following solution; mass of 0.85 mol of PbI_2 is 0.85×461 = 391.85 g, mass of 0.15 mol of MABr is 0.15×112 = 16.8 g, and mass of 1.00 mol of MAI is 1.00×159 = 159 g. Second, a ratio of comparison was used to calculate 1M of the solution as the followings; 1 mol of A is equal to 159 g. So, 1 M of A is equal to 159 g/L. Therefore, 0.065 M of A is equal to 10.34 g/L or 0.0103 g/ml. 0.0103 g/ml of MAI in IPA solution is a lowest ratio to dissolve in the solution.

Likewise the calculation of B and X_3. 1 mol of B is equal to 461 g. So, 1 M of B is equal to 461 g/L. Therefore, 0.065 M of B is 29.96 g/L or 0.0300 g/ml. Finally, 1 mol of X_3 is 391.85 + 16.8 = 408.65 g. So, 1 M of X_3 I equal to 408.65 g/L. Therefore, 0.065 M of X_3 is equal to 26.56 g/L or 26.56 mg/ml. According to $X_3 = (I_{0.85}Br_{0.15})_3$; 0.85 of PbI_2 is 0.85 × 26.56 = 22.57 mg/ml or 0.023 g/ml and 0.15 of MABr is 0.15 × 26.56 = 3.984 mg/ml or 0.004 g/ml.

As in the previous calculation, the PSCs with $MA_{1-x}Cs_xPb(I_{0.85}Br_{0.15})_3$ where x = 0.03, 0.05, 0.07 are similarly calculated as show in Table 2. Therefore, the structure of this condition is $MA_{1-x}Cs_xPb(I_{0.85}Br_{0.15})_3$ which A = $MA_{1-x}Cs_x$ [0.0629M], B = Pb [1M], and $X_3 = (I_{0.85}Br_{0.15})_3$ [1M].

Table2. Calculation of chemical substance in perovskite layer with $MA_{1-x}Cs_xPb(I_{0.85}Br_{0.15})_3$ with x = 0.03, 0.05, 0.07.

Ratio of MA	Mass (g/mol)	1M		0.0629M	
		g/L	g/ml	g/L	g/ml
0.97	159	154.23	0.1542	9.7011	0.0097
0.95	159	151.05	0.1510	9.5010	0.0095
0.93	159	147.87	0.1478	9.3010	0.0093
0.91	159	144.69	0.1446	9.1010	0.0091
Ratio of Cs	**Mass (g/mol)**	**1M**		**0.0629M**	
		g/L	**g/ml**	**g/L**	**g/ml**
0.03	260	7.8	0.0078	0.4906	0.0005
0.05	260	13	0.013	0.8177	0.0008
0.07	260	18.2	0.0182	1.1448	0.0011
0.09	260	23.4	0.0234	1.4719	0.0014
Ratio of I	**Mass (g/mol)**	**1M**		**0.0629M**	
		g/L	**g/ml**	**g/L**	**g/ml**
0.85	461	391.85	0.3918	-	-
Ratio of Br	**Mass (g/mol)**	**1M**		**0.0629M**	
		g/L	**g/ml**	**g/L**	**g/ml**
0.15	367	55.05	0.0550	-	-

The calculations of chemical substance in this condition are similarly calculated as the previous part as shown in Table 3. In addition, the structure of the PSCs with $MA_{0.97}Cs_{0.03}Pb(I_{1-y}Br_y)_3$ is A = $MA_{0.97}Cs_{0.03}$, B = Pb, and X_3 = $(I_{1-y}Br_y)_3$.

Table3. Calculation of chemical substance in perovskite layer with $MA_{0.97}Cs_{0.03}Pb(I_{1-y}Br_y)_3$ with y= 0.05, 0.10, 0.15, 0.20.

Ratio of MA	Mass (g/mol)	1M (g)		0.0629M (g)	
		g/L	g/ml	g/L	g/ml
0.97	159	154.23	0.1542	9.7010	0.0097
0.95	159	151.05	0.1510	9.5010	0.0095
0.93	159	147.87	0.1478	9.3010	0.0093
0.91	159	144.69	0.1446	9.1010	0.0091
Ratio of Cs	**Mass (g/mol)**	**1M (g)**		**0.0629M (g)**	
		g/L	**g/ml**	**g/L**	**g/ml**
0.03	260	7.8	0.0078	0.4906	0.0005
0.05	260	13	0.013	0.8177	0.0008
0.07	260	18.2	0.018	1.1447	0.0012
0.09	260	23.4	0.0234	1.4718	0.0015
Ratio of I	**Mass (g/mol)**	**1M (g)**		**0.0629M (g)**	
		g/L	**g/ml**	**g/L**	**g/ml**
0.95	461	437.95	0.4379	-	-
0.9	461	414.9	0.4149	-	-
0.85	461	391.85	0.3918	-	-
0.8	461	368.8	0.3688	-	-
Ratio of Br	**Mass (g/mol)**	**1M (g)**		**0.0629M (g)**	
		g/L	**g/ml**	**g/L**	**g/ml**
0.05	367	18.35	0.0184	-	-
0.1	367	36.7	0.0367	-	-
0.15	367	55.05	0.0550	-	-
0.2	367	73.4	0.0734	-	-

3.3.1 Preparation of TiO_2 layers

1) 1 ml of compact titanium dioxide (cp-TiO_2) was dissolved in 2 ml of ethanol. The solution was stirred for 20 hours in nitrogen filled glovebox. 400 μl of cp-TiO_2 solution was dripped and spun (3000 rpm, 30 s) on top of FTO, and then baked at 500°C for 30 mins in air.

2) 1 ml of mesoporous TiO_2 (mp-TiO_2) was dissolved in 7 ml of ethanol. The mp-TiO_2 solution was stirred for 20 hours. Then, 400 μl of mp-TiO_2 was coated on top of the cp-TiO_2 and spun (4000 rpm, 30 s), and then baked at 450°C for 30 mins in air.

3.3.2 Preparation of $MAPb(IBr)_3$

As the calculation previously described, the amount of chemical substance in this part is prepared for 12 samples of 3cm×3cm each.

1) PbI_2• (DMF:DMSO) adduct 2.305 g of PbI_2 was dissolved in 5 ml of Dimethylformadide (DMF) and Dimethyl sulfoxide (DMSO) under ratio 4:1 (v/v).

2) MAI•IPA adduct. 0.0620 g of MAI was dissolved in 6 ml of IPA.

3) MABr•IPA adduct. 0.0066 g of MABr was dissolved in 6 ml of IPA.

4) 0.2892 g of spiro-OMeTAD was dissolved in 4 ml of chlorobenzene. 0.260 g of Li was mixed in 0.5 ml of acetonitrile. After that, spiro-OMeTAD solution was mixed with Li solution.

5) All the solutions were stirred ~20 hours in the glovebox under 30% of the relative humidity.

3.3.3 Preparation of $MA_{1-x}Cs_xPb(I_{0.85}Br_{0.15})_3$ with x= 0.03, 0.05, 0.07, 0.09

As described in Table 2, the amount of chemical substance in this part is prepared for 12 samples of 3cm×cm each.

1) PbI_2•$PbBr_2$•(DMF:DMSO) adduct. 0.7837 mg of PbI_2 and 0.1101 mg of $PbBr_2$ were dissolved in 2 ml of Dimethylformadide (DMF) and Dimethyl sulfoxide (DMSO) under ratio 4:1 (v/v).

2) CsI•(DMF:DMSO) adduct. 0.0010 mg for 3% CsI was dissolved in 2 ml of Dimethylformadide (DMF) and Dimethyl sulfoxide (DMSO) under ratio 4:1(v/v).

3) CsI•(DMF:DMSO) adduct. 0.0016 mg for 5% CsI was dissolved in 2 ml of Dimethylformadide (DMF) and Dimethyl sulfoxide (DMSO) under ratio 4:1 (v/v).

4) CsI•(DMF:DMSO) adduct. 0.0022 mg for 7% CsI was dissolved in 2 ml of Dimethylformadide (DMF) and Dimethyl sulfoxide (DMSO) under ratio 4:1(v/v).

5) CsI•(DMF:DMSO) adduct. 0.0029 mg for 9% CsI was dissolved in 2 ml of Dimethylformadide (DMF) and Dimethyl sulfoxide (DMSO) under ratio 4:1 (v/v).

6) 97% MAI•IPA adduct. 0.0582 mg of MAI was dissolved in 6 ml of IPA.

7) 95% MAI•IPA adduct. 0.0570 mg of MAI was dissolved in 6 ml of IPA

8) 93% MAI•IPA adduct. 0.0570 mg of MAI was dissolved in 6 ml of IPA.

9) 91% MAI•IPA adduct. 0.0570 mg of MAI was dissolved in 6 ml of IPA.

10) 0.2892 g of spiro-OMeTAD was dissolved in 4 ml of chlorobenzene. 0.260 g of Li was mixed together in 0.5 ml of acetonitrile. After that, spiro-OMeTAD solution was mixed with Li solution.

11) All solutions were stirred ~20 hours in the glovebox under 30% of the relative humidity.

3.3.4 Preparation of $MA_{0.97}Cs_{0.07}Pb(I_{1-y}Br_y)_3$ with y= 0.05, 0.10, 0.15, 0.20

As shown in Table 3, the amount of chemical substance in this part is prepared for 12 samples of 3cm×cm each.

1) 97% MAI•IPA adduct. 0.0194 mg for MAI was dissolved in 6 ml for IPA.

2) CsI•(DMF:DMSO) adduct. 0.0010 mg for 3% CsI was dissolved in 3 ml of Dimethylformadide (DMF) and Dimethyl sulfoxide (DMSO) under ratio 4:1 (v/v).

3) PbI_2•$PbBr_2$•(DMF:DMSO) adduct. 0.8759 mg for 95% PbI_2 and 0.0367 mg for 5% $PbBr_2$ were dissolved in 3 ml of Dimethylformadide (DMF) and Dimethyl sulfoxide (DMSO) under ratio 4:1 (v/v).

4) PbI_2•$PbBr_2$•(DMF:DMSO) adduct. 0.8298 mg for 90% PbI_2 and 0.0734 mg for 10% $PbBr_2$ were dissolved in 3 ml of Dimethylformadide (DMF) and Dimethyl sulfoxide (DMSO) under ratio 4:1 (v/v).

5) PbI_2•$PbBr_2$•(DMF:DMSO) adduct. 0.7837 mg for 85% PbI_2 and 0.1101 mg for 15% $PbBr_2$ were dissolved in 3 ml of Dimethylformadide (DMF) and Dimethyl sulfoxide (DMSO) under ratio 4:1 (v/v).

6) PbI_2•$PbBr_2$•(DMF:DMSO) adduct. 0.7376 mg for 80% PbI_2 and 0.1468 mg for 20% $PbBr_2$ were dissolved in 3 ml of Dimethylformadide (DMF) and Dimethyl sulfoxide (DMSO) under ratio 4:1 (v/v).

7) 0.2892 g of spiro-OMeTAD was dissolved in 4 ml of chlorobenzene. 0.260 g of Li was mixed in 0.5 ml of acetonitrile. After that, spiro-OMeTAD solution was mixed with Li solution.

8) All the solutions were stirred ~20 hours in the glovebox under 30% of the relative humidity.

3.4 Deposition method for perovskite layer

The deposition processes for the PSCs in this work is a solution-based deposition method employing the two-step deposition as depicted in figure 14.

The two-step deposition method involves;

1) The chemical substance is separately prepared for PbX_2 solution and MAX solution.

2) The substrates are first dripped with PbX_2 solution, spin and annealed for structure formation.

3) After annealing, the substrates are dripped with MAX solution and spun.

4) Repeat step 3) again.

5) The substrates are annealed for the structure formation at high temperature depending on the properties of each chemical substance.

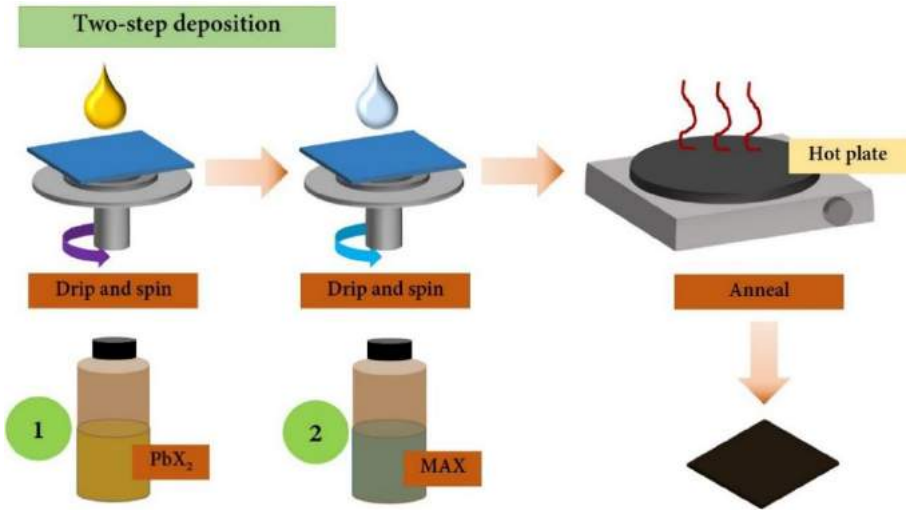

Fig.14 Solution-based deposition method.

3.5 Fabrication process of PSCs

1) The FTO glasses were treated in ultraviolet (UV)-Ozone chamber for 15 minutes prior to use.

2) The perovskite layer was prepared using the two-step method. The lead precursor solution was kept at 70°C for 30 minutes before use. After that, 200 μl of PbX_2 solution was spin-coated on top of mp-TiO_2 (3000 rpm, 20s). Then, the substrates were annealed at 70°C for 20 minutes.

3) 400 μl of MAX solution was spin-coated on top of PbX_2 layer (2000 rpm, 20 s). Then, MAX solution was spin-coated again on top of MAX layer (2000 rpm, 20 s) and followed by 75 μl chlorobenzene as the anti-solvent at 5 s after dripping MAX solution as depicted in figure 15.

4) The film was heated at 150°C for 15 minutes to eliminate the solvent in the film.

5) 200 μl of spiro-OMeTAD solution as the HTM was spin coated on top of perovskite layer (4000 rpm, 30 s) The samples were left in the dry box for 12 hours before putting on the gold contacts.

6) Gold was evaporated on top of the films as an electrode as shown in figure 16.

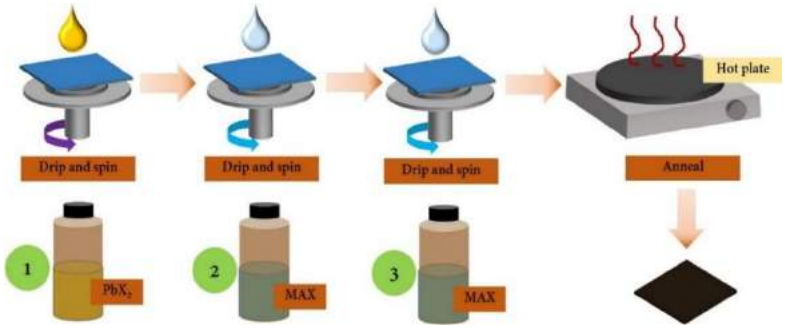

Fig.15 two-step deposition of perovskite layer.

Fig.16 Gold evaporation.

Chapter 4

Results and discussion

In this report, PSCs with mixed organic-inorganic cations – $MA_{1-x}Cs_xPb(I_{1-y}Br_y)_3$, where MA is methyl-ammonium, were fabricated by using the two-step spin-coating method. In this chapter, the results of I-V characteristic, absorbance, grain size, coloration of each condition are described.

4.1 I-V characteristics

The solar cell parameters including V_{oc}, J_{sc}, fill factor, and power conversion efficiency for the 0.06 cm^2 and 0.2 cm^2 active areas are reported. Forward and reverse voltage bias between -0.1 and 1.2 V were applied to the PSCs for the I-V measurements.

4.1.1 Open-circuit voltage (V_{oc})

Figure 17 shows the V_{oc} of the reference samples of both active areas. They are about 1 V with larger distribution for ther forward I-V measurements. In figures 18 (a) and (b), the V_{oc} of both cell areas with varying Cs concentrations are relatively constant around 1.0±0.05 V with narrower distribution for the reverse direction of I-V measurement. The V_{oc} of $MA_{1-x}Cs_xPb(I_{0.85}Br_{0.15})_3$ PSC with x = 0.03, 0.05, 0.07, 0.09 are more uniform than $MA_{0.97}Cs_{0.03}Pb(I_{1-y}Br_y)_3$ PSCs with y = 0.05, 0.10, 0.15, 0.20 as shown in figure 18(c)

and (d). Moreover, the V_{oc} in figure 18 (c) and (d) are slightly increase with 15%-20% of Br addition. The highest value of V_{oc} is obtained from 20% Br addition.

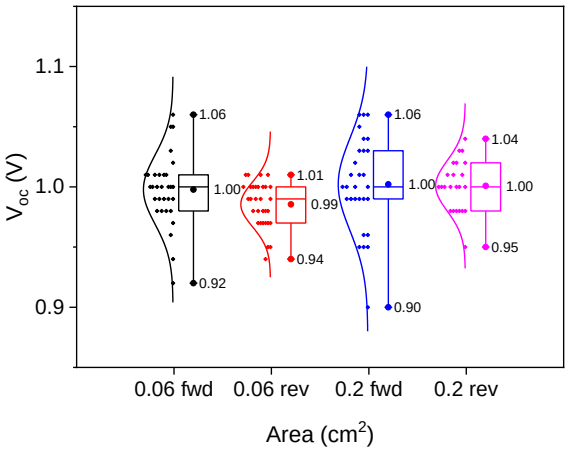

Fig.17 Open-circuit voltage of $MAPb(IBr)_3$ PSCs with 0.06 cm^2 and 0.2 cm^2 active areas.

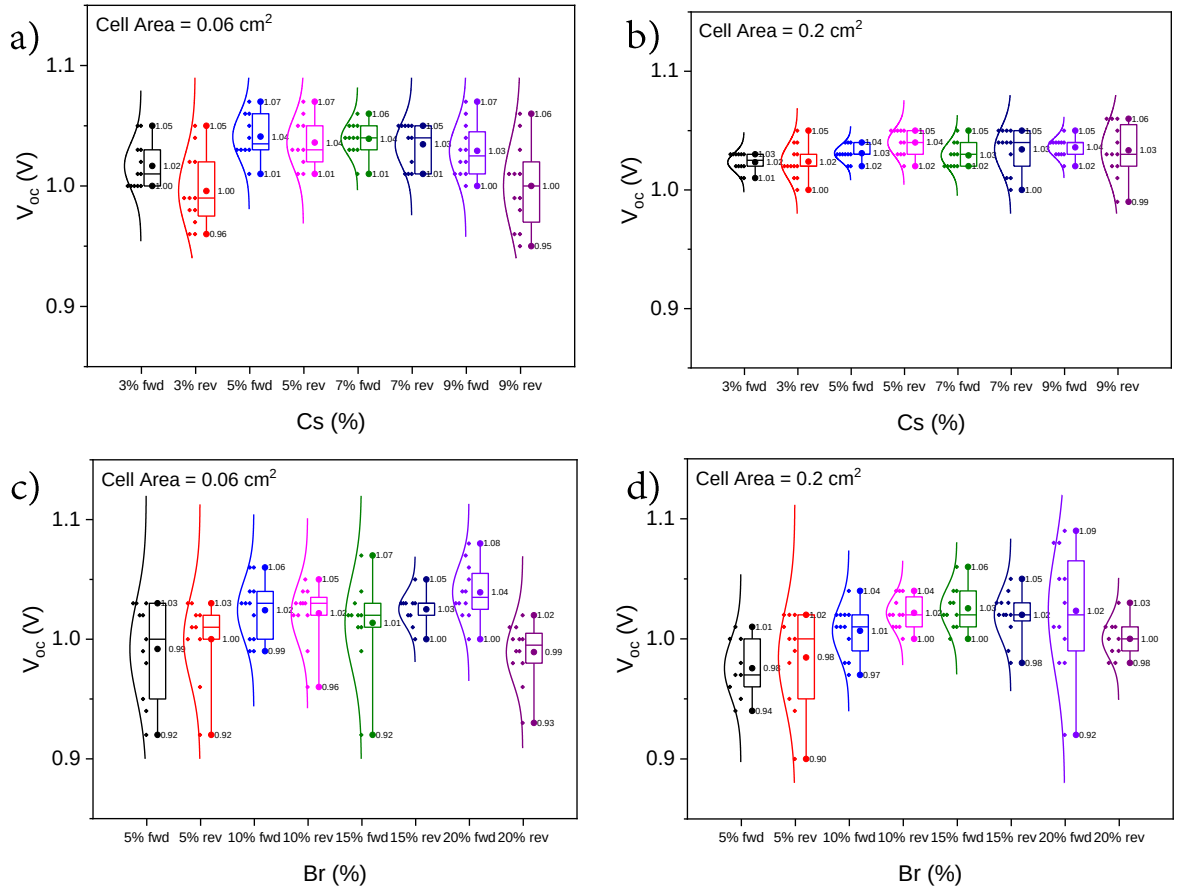

Fig18. Open-circuit voltage of PSCs **(a,b)** $MA_{1-x}Cs_xPb(I_{0.85}Br_{0.15})_3$ with x = 0.03, 0.05, 0.07, 0.09, **(c,d)** $MA_{0.97}Cs_{0.03}Pb(I_{1-y}Br_y)_3$ with y = 0.05, 0.10, 0.15, 0.20 for 0.06 and 0.2 cm^2 active areas.

4.1.2 Short-circuit current density (J_{sc})

The J_{sc} of the reference PSCs of 0.2 cm^2 active area are lower than that of the 0.06 cm^2 active area as shown in figure 19. In figures 20 (a) and (b), distribution of J_{sc} appears to be more uniform for Cs addition in 0.2 area cm^2 active area. However, the J_{sc} with Cs addition are relatively higher in 0.06 cm^2 active area. Large cell areas affect the decrease of J_{sc} because of recombination of electric charges due to more defects. For Br addition, 10% of Br seems to give higher J_{sc} as seen in figure 20(c) for 0.06 cm^2 active area. The J_{sc} from 20% Br addition drop dramatically as in figure 20(d) for 0.2 cm^2 active area.

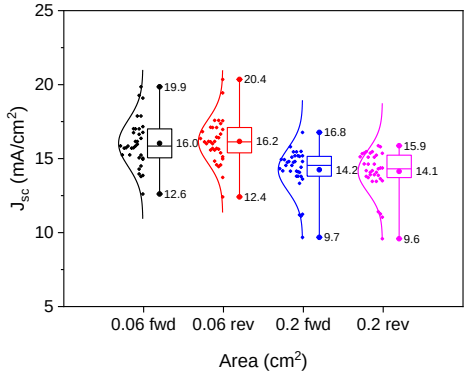

Fig.19 Short-circuit current density of $MAPb(IBr)_3$ PSCs with 0.06 cm^2 and 0.2 cm^2 active area.

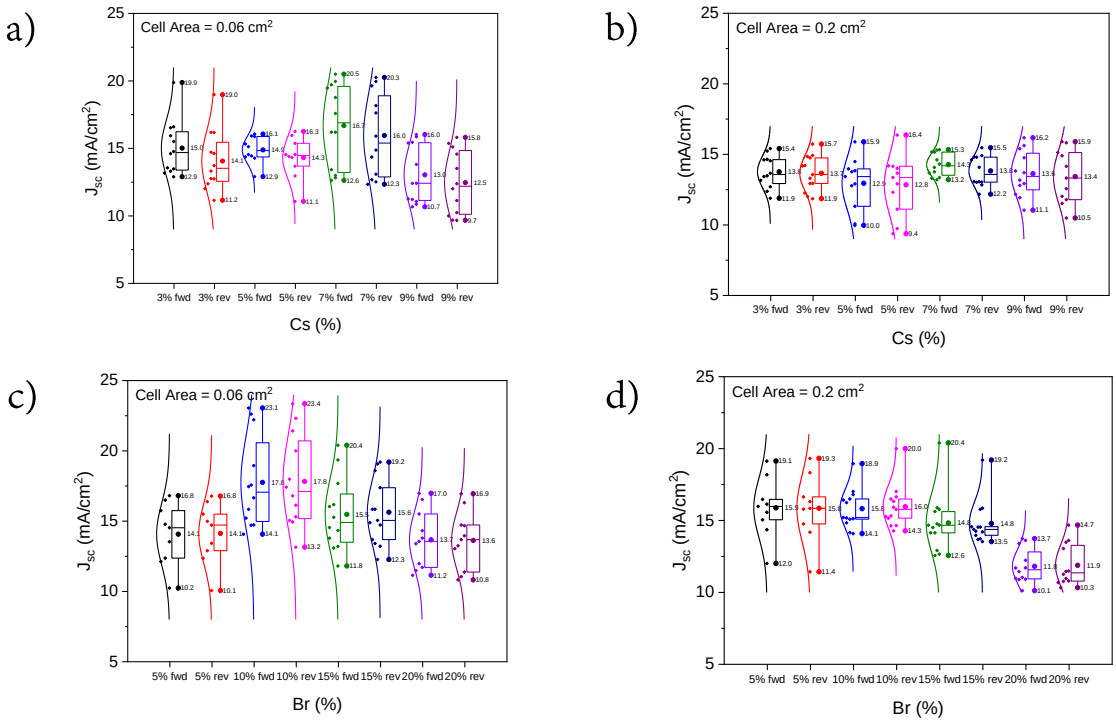

Fig20. Short-circuit current density of PSCs **(a,b)** $MA_{1-x}Cs_xPb(I_{0.85}Br_{0.15})_3$ with x = 0.03, 0.05, 0.07, 0.09, **(c,d)** $MA_{0.97}Cs_{0.03}Pb(I_{1-y}Br_y)_3$ with y= 0.05, 0.10, 0.15, 0.20 for 0.06 and 0.2 cm^2 active areas.

4.1.3 Fill factor

The higher fill factors are obtained from reverse direction of I-V measurements as shown in figure 21 and 22. FF is also are indication of the junction quality. Cs and Br addition seem to be indifferent in the distribution of FF.

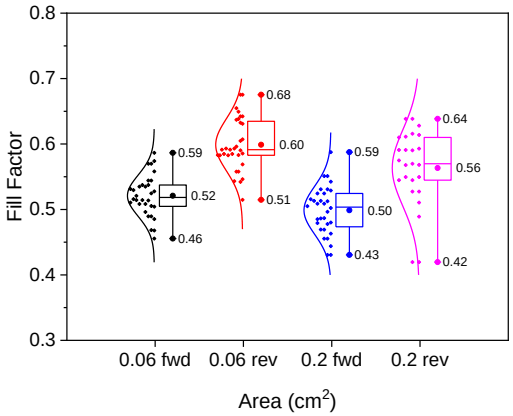

Fig.21 Fill factor of $MAPb(IBr)_3$ PSCs with 0.06 cm^2 and 0.2 cm^2 active areas.

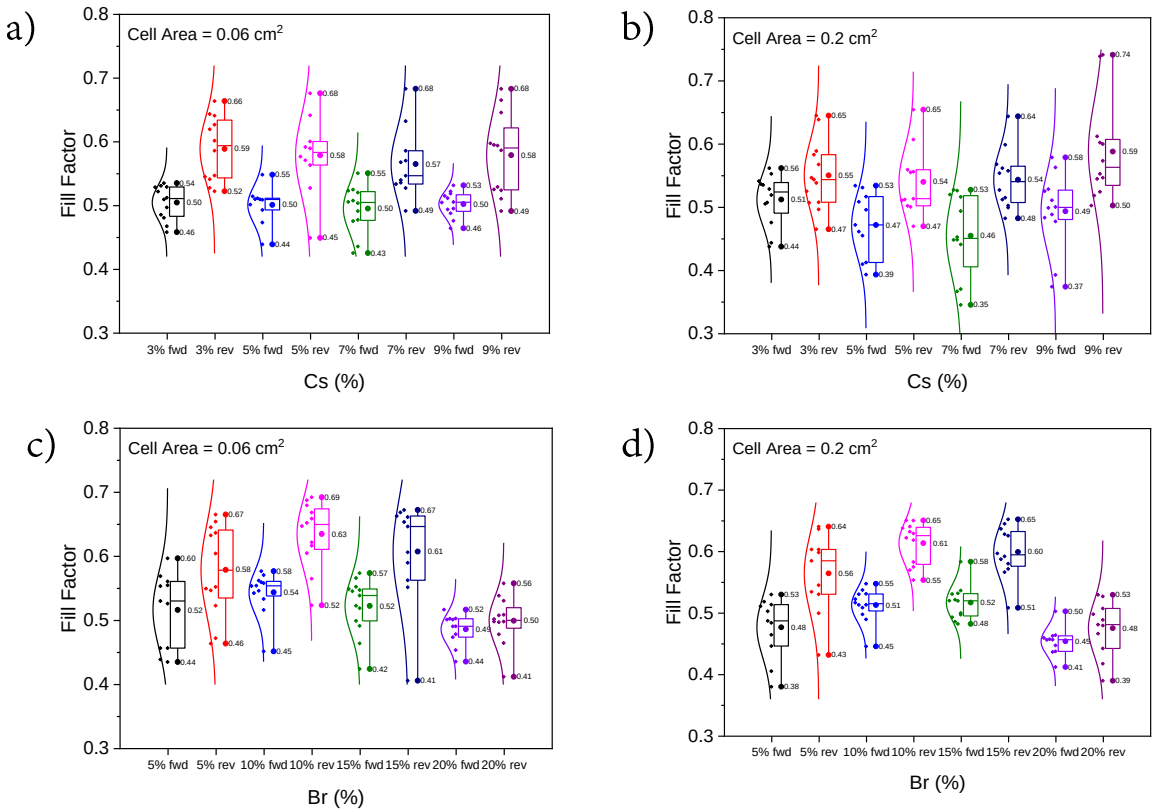

Fig.22 Fill factor of PSCs **(a,b)** $MA_{1-x}Cs_xPb(I_{0.85}Br_{0.15})_3$ with x = 0.03, 0.05, 0.07, 0.09, **(c,d)** $MA_{0.97}Cs_{0.03}Pb(I_{1-y}Br_y)_3$ with y = 0.05, 0.10, 0.15, 0.20 for of 0.06 and 0.2 cm^2 active areas.

4.1.4 Power conversion efficiency (PCE)

Figure 23 shows the PCE of the reference PSCs. It can be noticed that PSCs with 0.06 cm^2 active area have slightly higher PCE than the PSCs with 0.2 cm^2 active area. Also, reverse direction of I-V measurements yield higher PCE. Figures 24 (a) and (b) show that Cs addition does not quite affect to the PCE for both 0.06 cm^2 and 0.2 cm^2 active areas. On the other hand, Br addition affects the PCE of PSCs with $MA_{0.97}Cs_{0.03}Pb(I_{1-y}Br_y)$. The PCE is maximum at 10% of Br addition, as shown in figure 24(c).

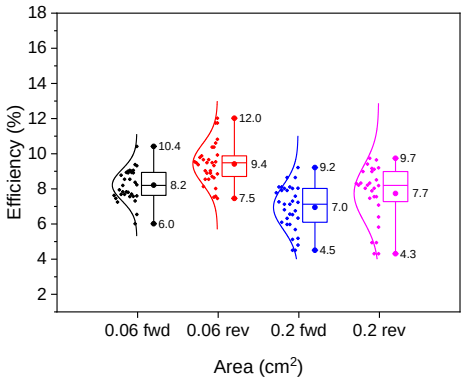

Fig.23 PCE of $MAPb(IBr)_3$ PSCs with 0.06 cm^2 and 0.2 cm^2 active areas.

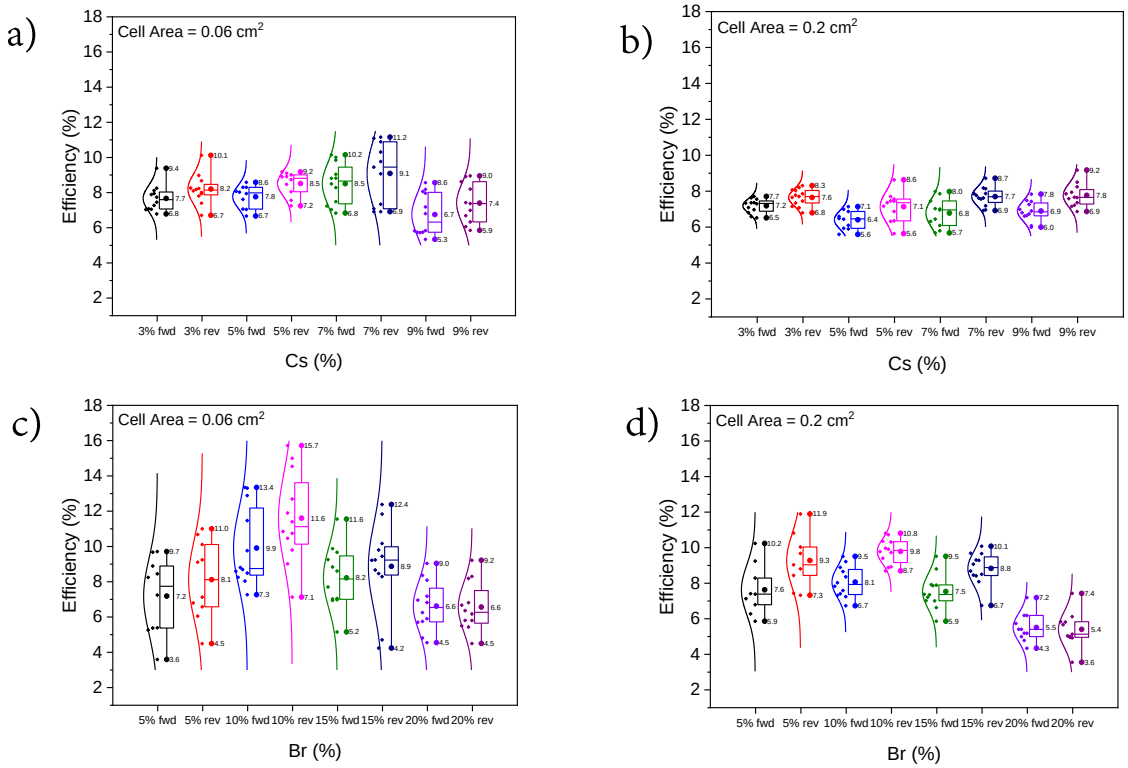

Fig.24 PCE of PSCs **(a,b)** $MA_{1-x}Cs_xPb(I_{0.85}Br_{0.15})_3$ with x = 0.03, 0.05, 0.07, 0.09, **(c,d)** $MA_{0.97}Cs_{0.03}Pb(I_{1-y}Br_y)_3$ with y = 0.05, 0.10, 0.15, 0.20 for of 0.06 and 0.2 cm^2 active areas.

The best of PSC of $MA_{0.97}Cs_{0.03}Pb(I_{1-y}Br_y)_3$ is with y= 0.10; PCE = 15.7%. V_{oc} = 1.04 V. J_{sc} = 23.35 mA/cm^2, FF = 64.74, R_{serie} = 2.363 Ω·cm^2 and R_{shunt} = 878.8 Ω·cm^2. The solar cell parameters of the best PSCs are summarized in Table 4.

Table4. Photovoltaic parameters of the best PSCs.

Condition	bias	V_{oc} (Volt)	FF	J_{sc} (A/cm^2)	PCE (%)
$MAPb(I_{0.85}Br_{0.15})$	rev	1.00	0.5903	20.35	12.0
$MA_{0.93}Cs_{0.07}Pb(I_{0.85}Br_{0.15})_3$	rev	1.05	0.5361	19.63	11.2
$MA_{0.97}Cs_{0.03}Pb(I_{0.90}Br_{0.10})_3$	rev	1.04	0.6474	23.35	15.7

4.2 Energy gap

As described in chapter 3, in some case, only the transmittance can be used to calculate the energy gap by plotting $(\alpha hv)^2$ vs. hv as shown in figure 25.

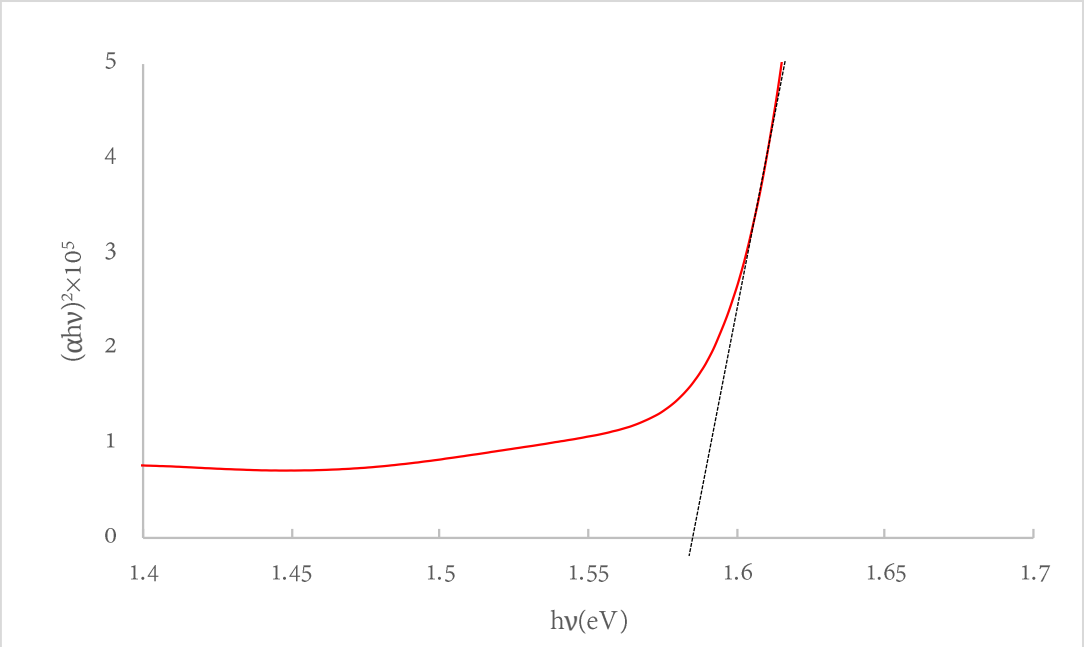

Fig.25 A plot of $(\alpha hv)^2$ and hv of PSCs with $MAPb(IBr)_3$.

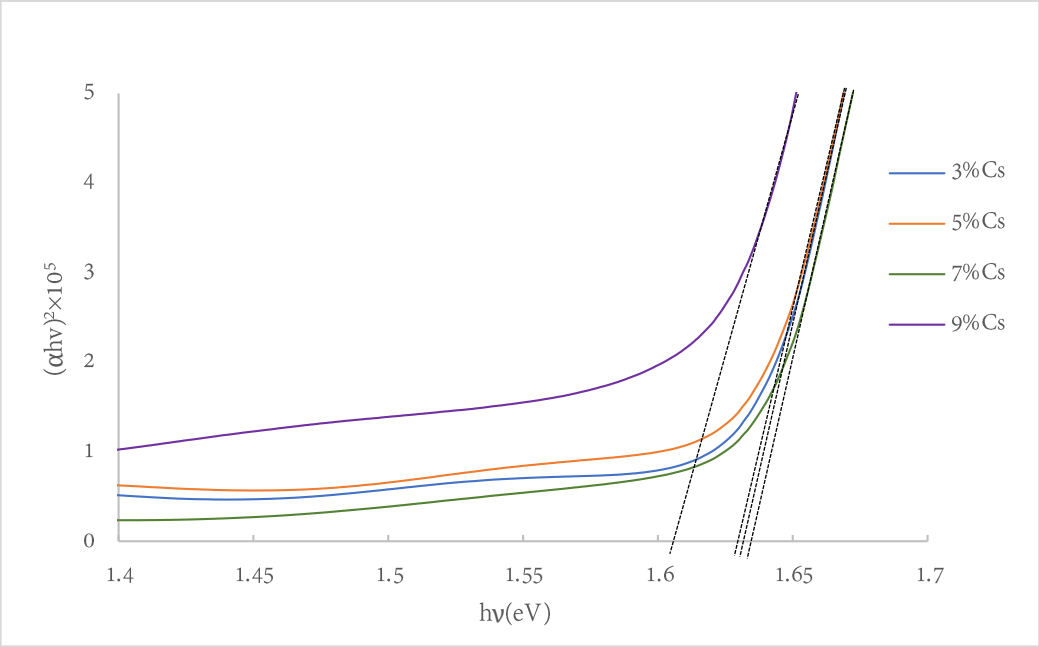

Fig.26 A plot of $(\alpha hv)^2$ and hv of PSCs with $MA_{1-x}Cs_xPb(I_{0.85}Br_{0.15})_3$ where x = 0.03, 0.05, 0.07, and 0.09.

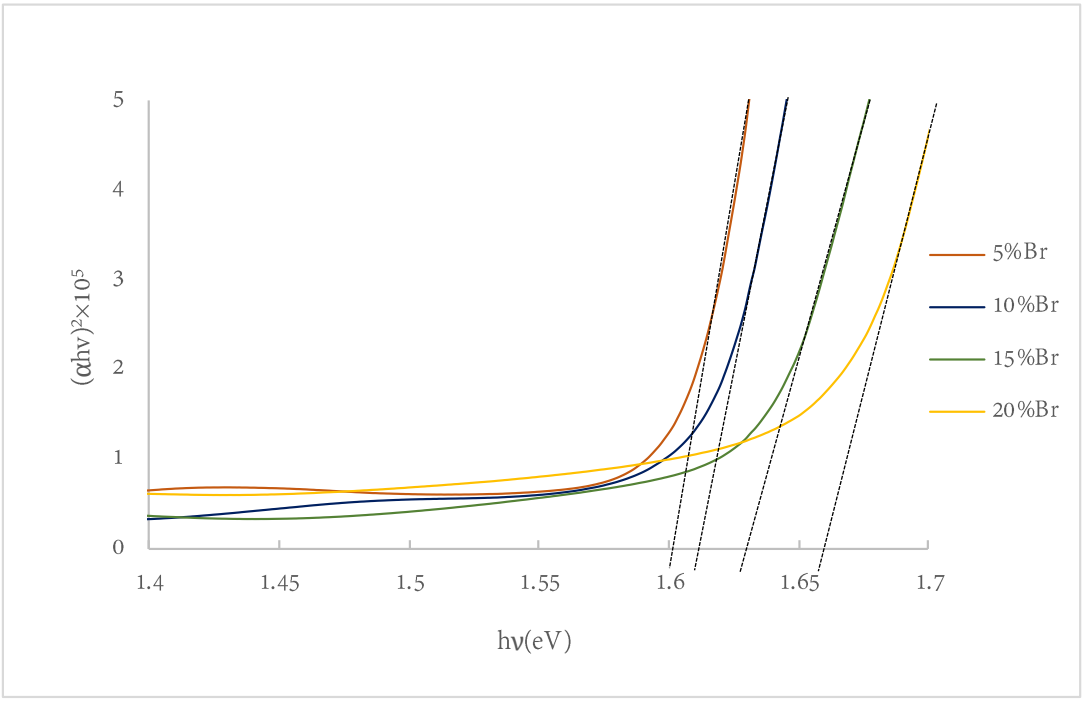

Fig.27 A plot of $(\alpha hv)^2$ and hv of PSCs with $MA_{0.97}Cs_{0.03}Pb(I_{1-y}Br_y)_3$ where y = 0.05, 0.10, 0.15, and 0.20.

The concentrations of Cs seem not to affect the energy gap value except when Cs is 9% as shown in figure 26. On the other hand, the energy gap of PSCs with Br addition are noticeably increased when the Br concentrations

are increased from 5, 10, 20% as shown in figure 27. The values of the E_g of PSCs with Br concentrations are summarized in Table 5.

Table5. Energy gap of PSCs with additions of Br.

Condition	Energy gap (eV)
$MAPbI_3$	1.58
$MA_{0.97}Cs_{0.03}Pb(I_{0.85}Br_{0.05})_3$	1.60
$MA_{0.97}Cs_{0.03}Pb(I_{0.85}Br_{0.10})_3$	1.61
$MA_{0.97}Cs_{0.03}Pb(I_{0.85}Br_{0.15})_3$	1.63
$MA_{0.97}Cs_{0.03}Pb(I_{0.85}Br_{0.20})_3$	1.66

4.3 Absorbance

The plot of absorbance of reference PSC is illustrated in figure 28. The absorption threshold is approximately 780 nm corresponding to 1.59 eV. The knee around 750 nm is due to the residue if PbI_2 in the film.

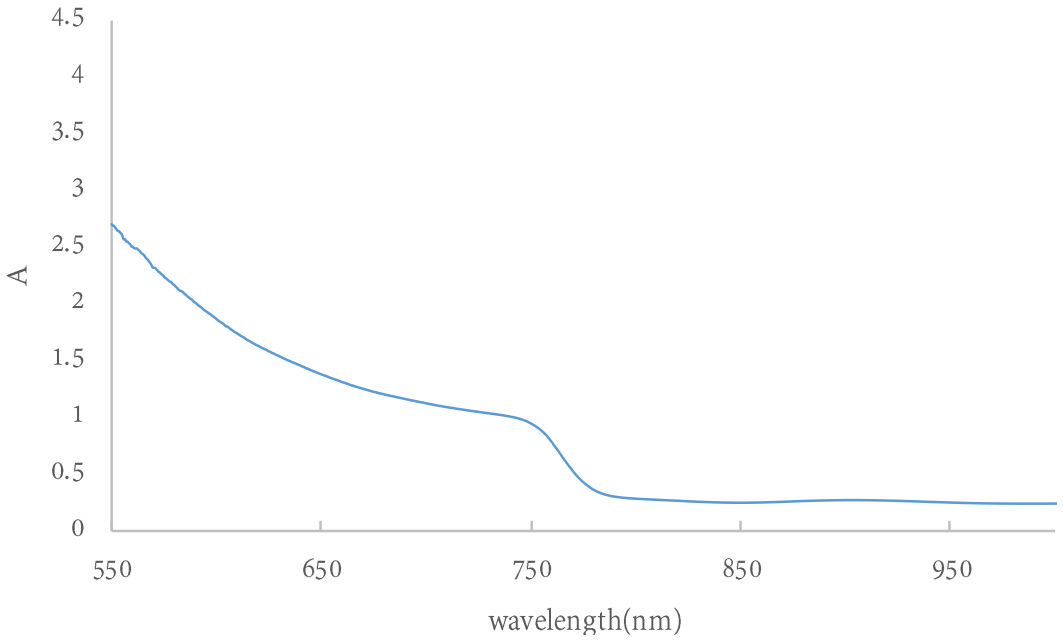

Fig.28 A plot of absorbance of PSC with $MAPb(I_{0.85}Br_{0.15})_3$.

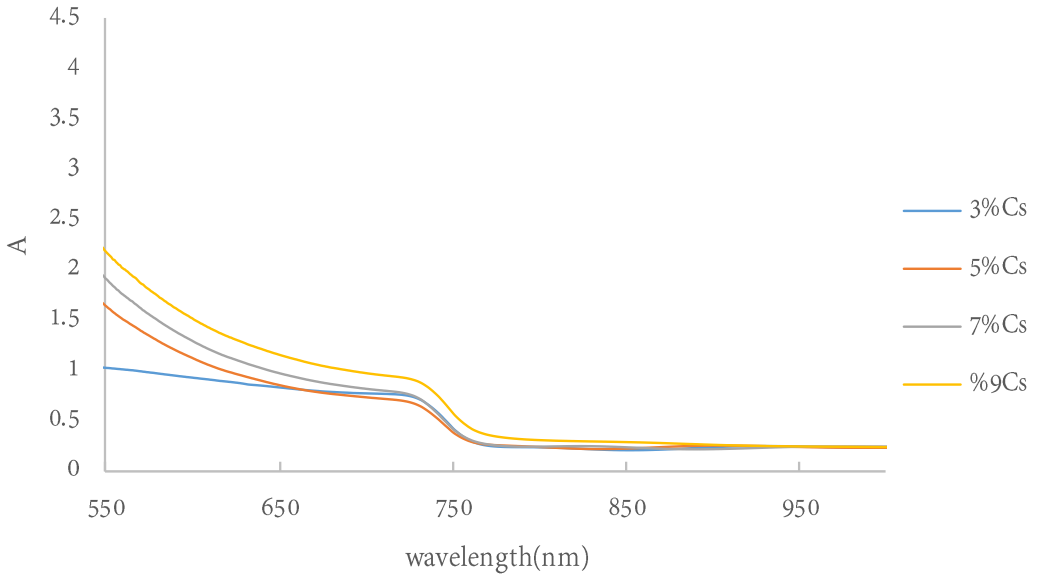

Fig.29 A plot of absorbance of PSCs with $MA_{1-x}Cs_xPb(I_{0.85}Br_{0.15})_3$ where x = 0.03, 0.05, 0.07, and 0.09.

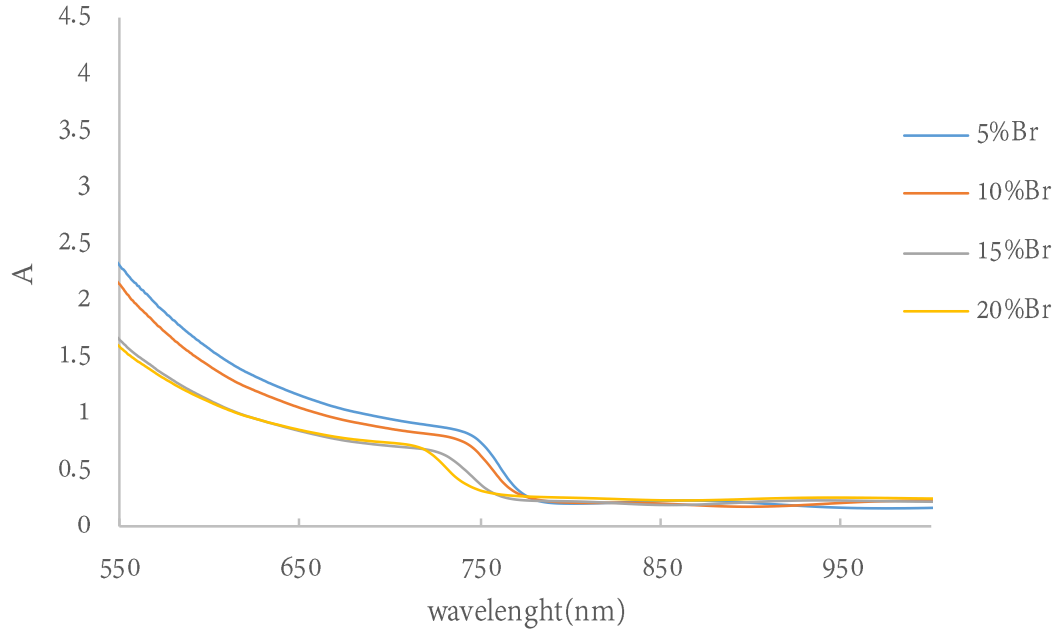

Fig.30 A plot of absorbance of PSCs with $MA_{0.97}Cs_{0.03}Pb(I_{1-y}Br_y)_3$.

The absorption thresholds for the PSCs with Cs additions seem not to be different for $x < 0.09$ as shown in figure 29. On the other hand, the absorption threshold clearly shows blue shift when the Br concentration increases as illustrated in figure 30.

4.4 Surface morphology

4.4.1 Cs addition

Figure 31 shows the surface morphology from SEM for the reference PSC. The grain sizes are in the order of a few hundreds nanometers. The grain are compact and show no pinholes. Figure 32 (a-d) are the surface by SEM (30,000x) with varying concentration of Cs; $MA_{1-x}Cs_xPb(I_{0.85}Br_{0.15})$ when x = 0.03, 0.05, 0.07, 0.09. The increasing of Cs concentration does not affect the grain size of absorber, but the grain size appears to be slightly smaller than that of the reference one. There are also some pinholes observed in the film with Cs = 9%.

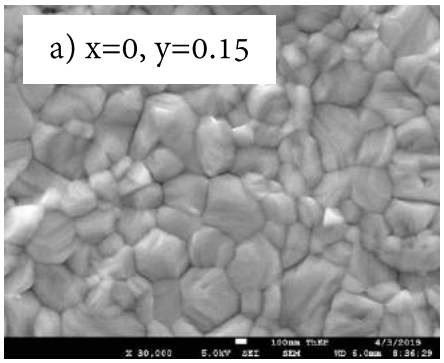

Fig.31 SEM image of the surface of PSCs with $MAPb(I_{0.85}Br_{0.15})_3$ a reference sample.

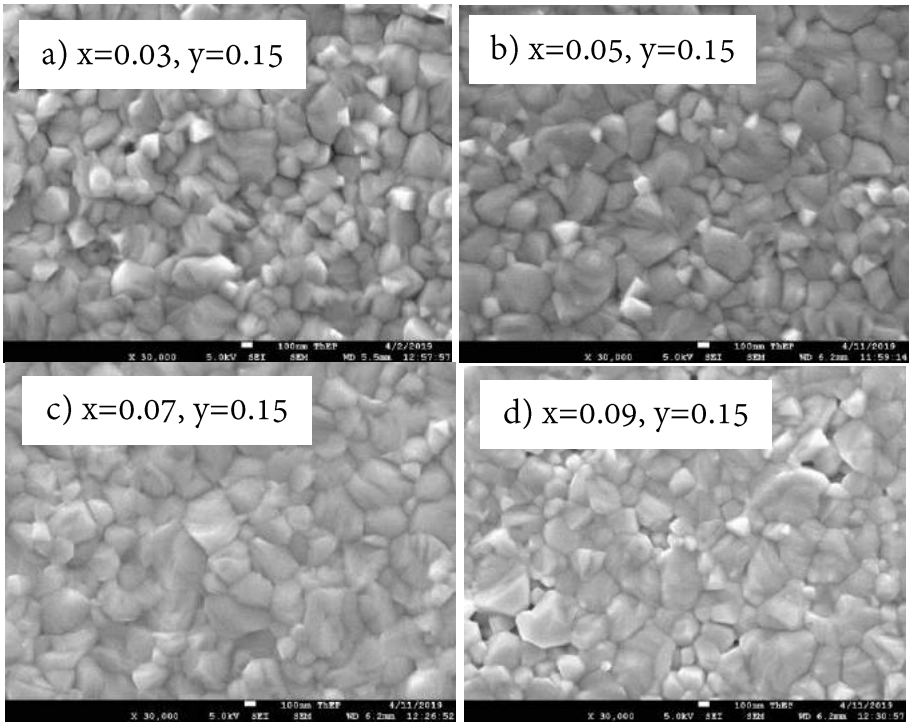

Fig.32 SEM image (×30,000) of a) absorbers with $MA_{0.97}Cs_{0.03}Pb(I_{0.85}Br_{0.15})$, b) Absorbers with $MA_{0.95}Cs_{0.05}Pb(I_{0}85Br_{0.15})$, c) Absorbers with $MA_{0.93}Cs_{0.07}Pb(I_{0.85}Br_{0.15})$, d) Absorbers with $MA_{0.91}Cs_{0.09}Pb(I_{0.85}Br_{0.15})_3$.

4.4.2 Br addition

The SEM images (30,000x) of absorbers with varying concentration of Br are compared in figure 33. The grain sizes seem to be affected by the Cs addition as shown in figure 33 (b) and (c) rather than Br. Moreover, grain boundaries are increased by increasing concentration of Cs. The J_{sc} value will be decreased by increasing of grain boundary.

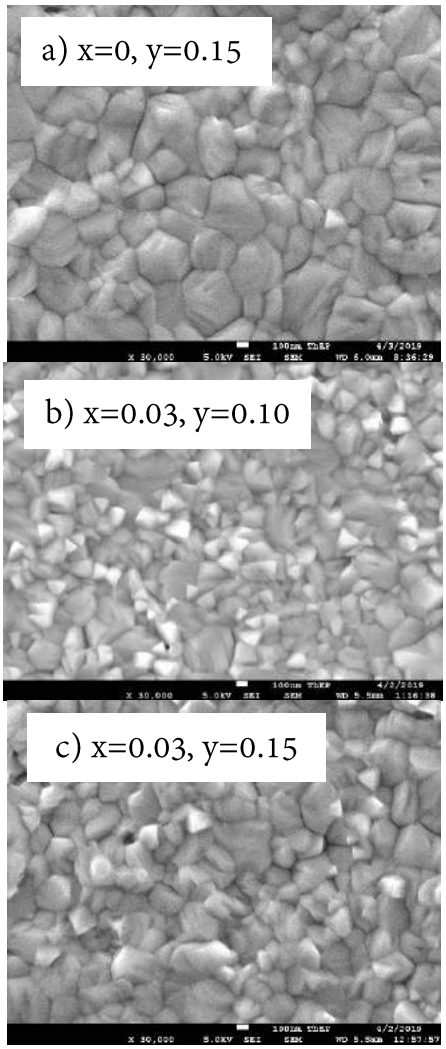

Fig.33 SEM images (30,000x) of a) PSCs with $MAPb(IBr)_3$, b) PSCs with $MA_{0.97}Cs_{0.03}Pb(I_{0.90}Br_{0.10})_3$, c) PSCs with $MA_{0.97}Cs_{0.03}Pb(I_{0.85}Br_{0.15})_3$.

4.5 Coloration of the absorbers

The absorbers with additions of Cs and Br have stabilized coloration when compared with the reference $MAPb(IBr)_3$. For 5 weeks of observation, the color of absorbers are shown in figure 34. The films were kept in vacuum chamber. As shown in figure 34, the absorbers can preserve coloration for 5 weeks. After that, the color of the films slightly changed. Finally, the absorbers with $MAPb(I_{0.85}Br_{0.15})_3$ degraded to yellowish shade in week 5.

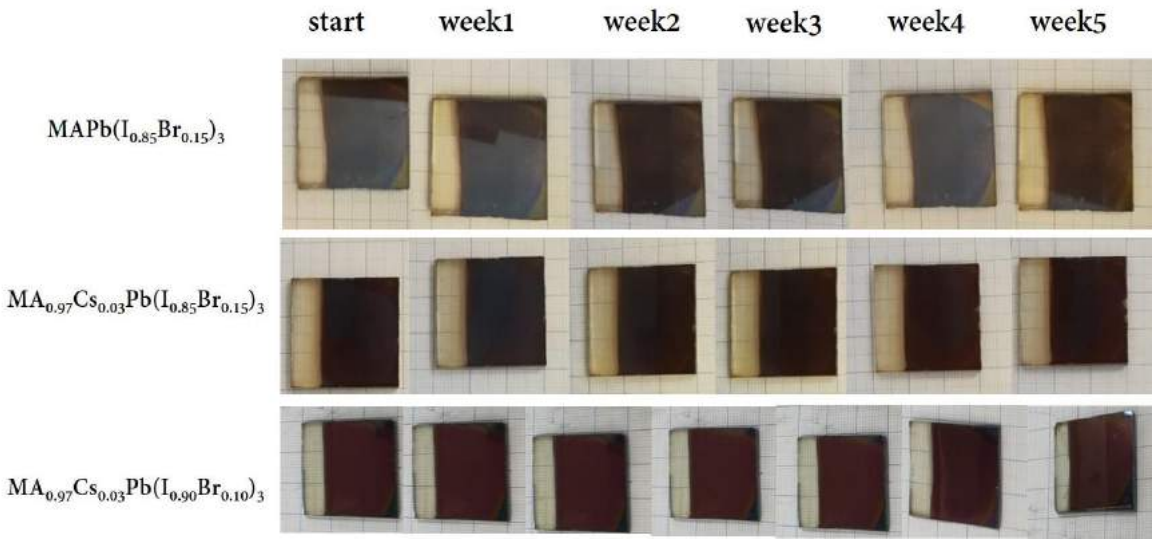

Fig.34 The coloration of absorbers with $MACsPb(I_{1-y}Br_y)_3$ and $MA_{1-x}Cs_xPbI_3$ over 5 weeks.

Chapter5

Conclusion

The PSCs with Cs and Br additions in the light harvesting layer; $MA_{1-x}Cs_xPb(I_{1-y}Br_y)_3$ with x=0.03, 0.05, 0.07, 0.09 and y=0.05, 0.10, 0.15, 0.20 were fabricated by the two-step spin-coating method.

The addition of Cs does not quite affect the absorption threshold of the absorbers except when Cs content is up to 9%. In contrast, the absorption threshold shows blue shift when Br content is increased. The Cs additions cause the grain size of the absorber smaller than the ones without Cs.

Moreover, the excess additions of Br and Cs are disadvantages, e.g., the films become opaque. The thermal treatment and time to stir are important to formation of the crystal structure. The PCE with 3% Cs addition is higher than other concentration in $MA_{1-x}Cs_xPb(I_{0.85}Br_{0.15})_3$.

Finally, the best solar cell parameters value is obtained by the PSCs with $MA_{1-x}Cs_xPb(I_{1-y}Br_y)_3$ when x = 0.03 and y = 0.10 with V_{oc} = 1.04 V, J_{sc} = 23.4 mA/cm^2, fill-factor = 64.7% and PCE = 15.7%.

References

[1] Martin A. Green, Anita Ho-Baillie, Henry J. Snaith. The emergence of perovskite solar cells. Nature Photonics 8 (July 2014): 506-514.

[2] Im. J-H, In-Hyuk Jang, Norman Pellet. Growth of $CH_3NH_3PbI_3$ cuboids with controlled size for high-efficiency perovskite solar cells. Nature Nanotechnology (August 2014): 1-6.

[3] J-W Lee, N-A Park. Two-step deposition method for high-efficiency perovskite solar cells. MRS Bulletin (August 2015): 654-659.

[4] Pablo P. Boix, Kazuteru Nonomura. Current progress and future perspectives for organic/inorganic perovskite solar cells. Materials Today 17 (January 2014): 16-23.

[5] X. Li et al. A vacuum flash-assisted solution process for high-efficiency large-area perovskite solar cells. Science (June 2016): 1-9.

[6] Eya Belarbi, Marta Valles-Pelarda. Transformation of PbI_2, $PbBr_2$, $PbCl_2$ salts into $MAPbBr_3$ perovskite by halide exchange as an effective method for recombination reduction. Royal society of chemistry. (March 2017): 1-9.

[7] Jangwon Seo, Jun Hong Noh and Sang Il Seok. Rational strategies for efficient perovskite solar cells. American Chemical society. (March 2016): 1-11.

[8] Osbel Almora, L. Vaillant-Roca and Germa Garcia-Belmonte. Perovskite solar cells: A brief introduction and some remark. Artculo De Revision. (June 2016): 1-11.